Kazimierz Gwizdała
Politechnika Gdańska

Moust Jacobsen
University of Aalborg

BEARING CAPACITY AND SETTLEMENTS OF PILES

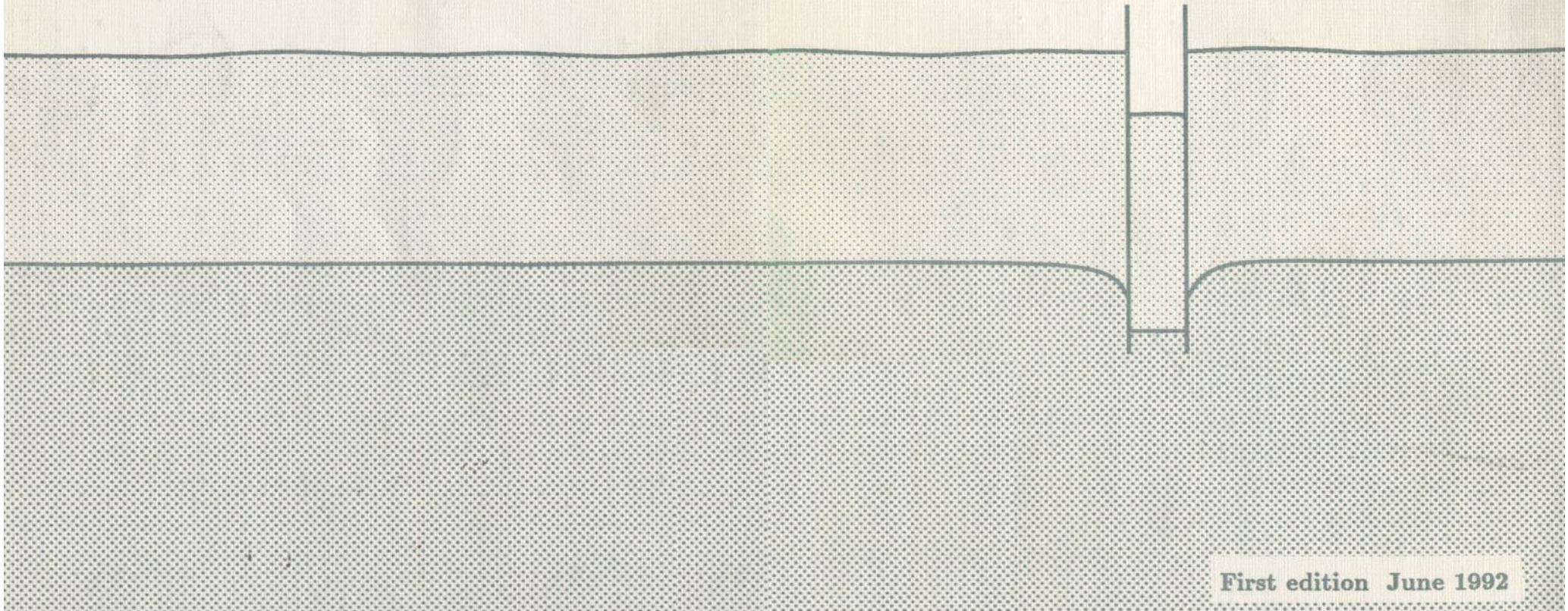

First edition June 1992

First Edition

BEARING CAPACITY AND SETTLEMENTS OF PILES

June 1992

Kazimierz Gwizdała
Politechnika Gdańska

Moust Jacobsen
University of Aalborg

Printed in Denmark by
Centertrykkeriet, Aalborg University
ISBN 87-88787-10-9

Preface

This textbook is a result of the mutual cooperation between the technical University in Gdansk, Poland and the University of Aalborg, Denmark, which has now been running for 6 years.

The authors have tried to combine the best traditions from the two countries in this book. The time will show if they have succeeded.

June 1992

Kazimierz Gwizdała
Politechnika Gdańska

Moust Jacobsen
University of Aalborg

Contents

CONTENTS

Chapter 1

Introduction

This book deals with site investigations, installation, and calculations of bearing capacity and settlement of a single pile. Anyway, before going into details it is useful to make it clear that there are big differences between analyses of piles and other constructions in soil.

1.1 Point resistance

The estimation of the ultimate bearing capacity for a shallow footing is easily done by the theory of plasticity (Fig. 1.1a). When a circular footing with diameter D is situated in a certain depth d below the surface, the theory of plasticity can be used to calculate a depth factor, when assuming a plastic zone from footing to the soil surface.

But when d/D gets bigger (for instance by driving a pile), elastic movements in the soil make it more and more difficult for the plastic zone to develope from pile tip to soil surface and for a certain value of d/D ($d/D \approx 3-5$) the plastic zone is only located to the lower part of the pile.

The magnitude of pore pressure developed in the plastic zone in a normally consolidated clay should be $\Delta u \sim 0.6 \cdot s_u$ and in a preconsolidated clay much lesser or even negativ. But during installation of the pile the pore pressure development in the plastic zone and along the pile shaft is totally dominated by the volume displacement from the pile and can exceed $5-7 \cdot s_u$. Meyerhof (1976), Randolph (1983). During consolidation the

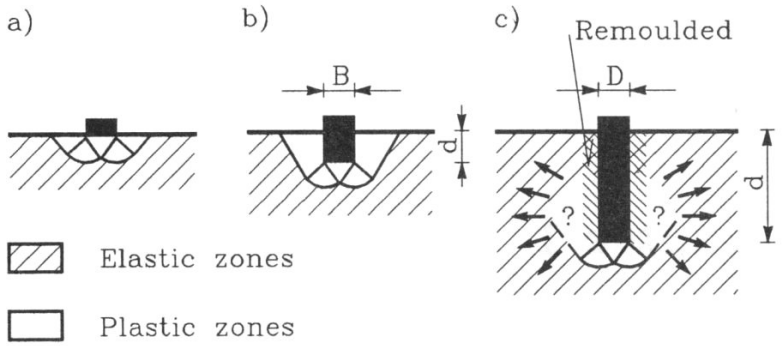

Figure 1.1: Elastic and plastic behaviour of soil below foundations and around piles.

$5 - 7 \cdot s_u$. Meyerhof (1976), Randolph (1983). During consolidation the effective stresses increases.

So — when analysing the point resistance of a pile — the method of installation and the type of pile, which causes the volume displacement, must be taken into account, and the analysis should be based on a elastic-plastic method, as proposed by Vesic (1975) and Kulhawy (1984).

If the pile is driven into a frictional material the problem is even bigger since displacements are followed by volume increments.

Today it is not possible to make a plastic-elastic analysis.

1.2 Shaft resistance

The shaft resistance developes in a narrow remoulded zone between the surface of the pile and the normal soil with elastic-plastic behaviour, Fig. 1.2. It depends in the characteristics of soil (sand- and clay-contents, maximum grain size) and the material surface (steel or concrete, rough or smooth). In the installation phase water could smoothen the surface and, furthermore, reduce the shaft resistance.

The shaft resistance will increase after installation, because the soil will regenerate. The regeneration depends on the soil and the stress history.

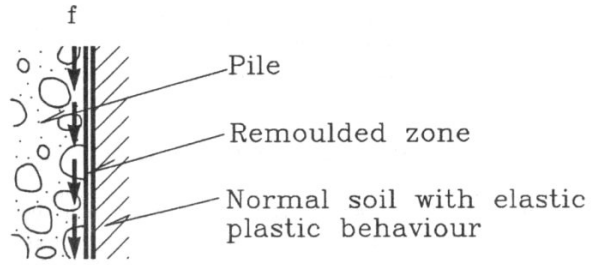

Figure 1.2: Sliding along concrete or steel surfaces.

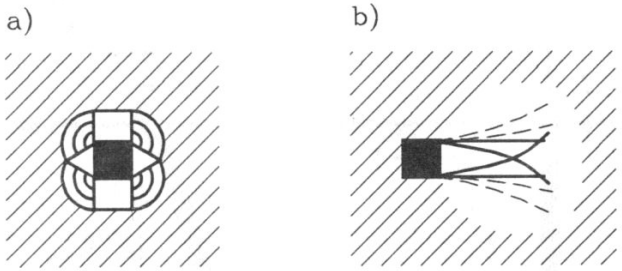

Figure 1.3: Horizontal movement around a pile.
a) in clay (undrained case) b) in sand (drained case)

The basic understanding of development of shaft resistance and regeneration can easily be achieved from tests in Casagrandes shear box. Scale effects depend on the grain size and surface roughness of pile materials and are normally unimportant.

1.3 Horizontal resistance

The horizontal resistance in clay (undrained case) can be estimated by the theory of plasticity, Fig. 1.3a, since the volume in the plastic zone is constant.

But in sand it is not possible to describe a closed rupture figure because

logaritmic spirals should be used. In reality it is even more complicated because the volume increments in the plastic zone must be followed by elastic deformations in the surrounding soil.

1.4 Movements of a single pile

For a *normal, shallow foundation* the settlement can be estimated using equations for loading an elastic half space. The main reason is that the settlements are very small compared with the size of the foundation. When the settlements exceed a certain value, pile foundation will be used instead.

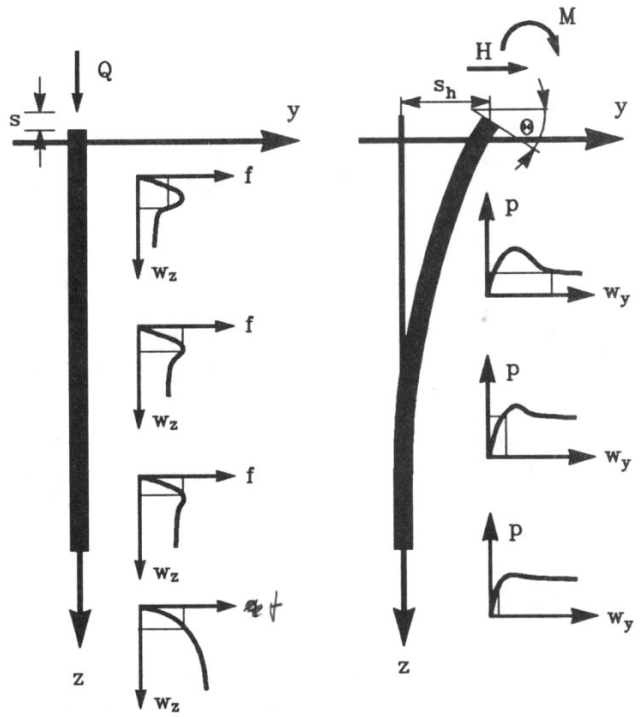

Figure 1.4: Settlement and movements of an elastic pile.

For *a pile* with a diameter which is small compared with the length or width of the foundation, the settlement curve is not linear, and more sophisticated methods have to be used. Furthermore, some part of the vertical load is carried by the shaft and spread out into the soil from the pile surface, another part of the vertical load is carried by the pile tip, and a horizontal load must spread out horizontally from the shaft.

The vertical settlement s of the pile top is calculated in two steps:

i) Settlement along the pile shaft.

By laboratory testing some so-called $f - z$ (or $t - z$ curves) can be constructed. They reflect the vertical movements w_z in the narrow zone along the pile surface.

It is normally assumed that the settlements along the pile are dominated by the narrow zone, but some authors proposed to take settlement in the undisturbed soil into account too.

The elasticity of long piles causes progressive failure along the shaft.

ii) Vertical settlement of pile tip.

The load-settlement curve for the pile tip is called a $q - z$ curve. It cannot be estimated from oedometer tests, but must still be studied by back-calculation of pile tests by use of $f - z$ curves or by direct measurements.

The $q - z$ curves then reflect the deformations in the soil beneath the pile tip and the vertical movement w_z of the pile tip.

In clay the initial tangent to the $q - z$ curve can be calculated from the theory of elasticity in rather close accordance with observations.

But normally the curved part of the $q - z$ curves should be used for settlement calculations and it is necessary to find a mathematical description of the curve. (As for instance the "hyperbolic type", formula (6.2).)

The horizontal movement of the pile top s_h and the distorsion θ can be calculated by a Winkler model, based on the so-called $p - y$ curves. The $p - y$ curves can be estimated by laboratory tests. They reflect the deformations in the soil around the pile and the horizontal movements w_y

of the shaft. In clay the deformations corresponding to a small horizontal load on a pile may be calculated from the theory of elasticity and the initial tangent to the $p - y$ curve can then be estimated.

It is important to point out that horizontal and vertical movements along the shaft may interact and the displacements grow bigger.

1.5 Danish Code

In Danish practice the so-called "geostatical" calculation mentioned above has no good reputation and normally pile driving formulas, PDA-measurements and pile loading tests are recommended.

Since this note concentrates on the "geostatical" calculation the following formulas from the Danish code should be mentioned:

The bearing capacity Q consists of a point load Q_p and shaft resistance Q_m:

$$Q = Q_m + Q_p$$

where Q_p can be derived from the following formulas:

In clay: $Q_p = 9\ s_u\ A_p$
in moraine clay the factor can be 18. This reflects the influence of the stiffness of the soil on the cavity expansion.

In sand: $Q_p = 2\ N_q\ q'_v \cdot A_p$
it is not mentioned in the last edition of the code, since it gives an increasing bearing capacity with any depth. (Compare Fig. 1.1 b and c), and it is postulated (Meyerhof, 1976) that from a certain depth d_c ("critical depth") Q_p in sand is constant.

In clay: $Q_m = m\ r\ s_u\ A_m = \alpha\ s_u\ A_m$
where m depends on the material: $m = 0.7$ for steel and $m = 0.8$-1 for concrete. r is a regeneration factor. Normally r is assumed to be 0.4, at least for moraine clay, and 1 for normally consolidated clays. α is then varying between 0.3 for moraine clay and 1 for normally consolidated clay.

In sand: $Q_m = N_m \cdot q'_{v,m} \cdot A_m$
where $N_m = 0.6$ in compression and 0.2 in extension.

These formulas are developed for normally small piles, but as this note shows, in rather close agreement even with the calculation methods for big diameter offshore piles.

1.6 Polish Code

In Polish practice the so-called "geostatical" calculations and loading tests are recommended.

The bearing capacity Q is the sum of a point resistance Q_p and shaft resistance Q_m:

i) in compression

$$Q = Q_p + Q_m = S_p \cdot q \cdot A_p + \sum S_{si} \cdot f_i \cdot A_{mi}$$

ii) in uplift

$$Q^t = \sum S_i^w \cdot f_i \cdot A_{mi}$$

where i refers to the number of the layer, q is unit base resistance, f is unit shaft resistance and S_p, S_s, S^w are engineering factors.

Base resistance

The unit resistance of *non-cohesive soils* at the pile base, q, is specified in Table 1.1, depending of type of soil and density index I_D or liquidity index

I_L. The influence of pile base diameter on q (and d_c) should be taken into account for *medium dense* and *dense non-cohesive soils* (Figures 1.5a and 1.5b).

Table 1.1. Values of unit ultimate resistance of non-cohesive soils at the pile base. Unit base resistance q (kPa).

Soil type	Density index			
	$I_D = 1.00$	$I_D = 0.67$	$I_D = 0.33$	$I_D = 0.20$
Gravel, sand-gravel mix	7750	5100	3000	1950
Coarse and medium sand	5850	3600	2150	1450
Fine sand	4100	2700	1650	1050
Silty sand	3350	2100	1150	700

	Liquidity index			
	$I_L < 0$, $w \simeq 0$	$I_L = 0$, $w = w_p$	$I_L = 0.50$	$I_L = 0.75$
Loamy gravel, gravel-sand-clay mix	4150	2750	1650	850
Loamy sand, sandy loam, loam, silty loam	2750	1950	850	450
Firm sandy loam, firm loam, form silty loam, sandy clay, clay, silty clay	2800	1950	800	400
Sandy silt, silt	1850	1250	500	250

q is specified for depths, d equal to or exceeding the critical depth $d_{ci} = d_c^o\sqrt{D_i/D_o}$, where $d_c^o = 10\ m$, $D_o = 0.4\ m$ and D_i is the actual base diameter. Linear interpolation should be adopted to determine values of q for depths less than d_c, with zero taken as the value of q for the initial ground level, Fig. 1.5 a).

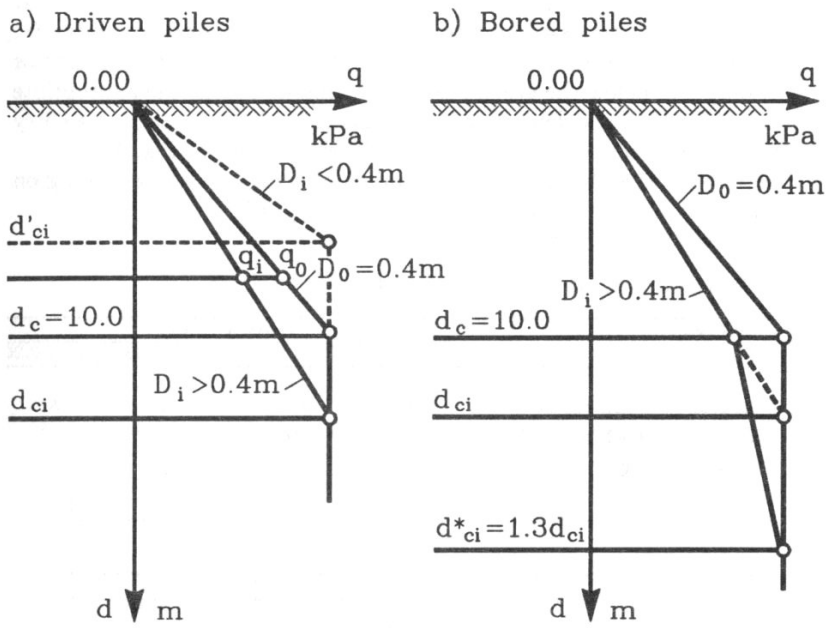

Figure 1.5: Interpolation of unit base resistance. (Non-cohesive soils)

The critical depth should be increased by 30% in case of bored piles, $d_{ci}^* = 1.3d_{ci}$. The ultimate resistance of soil under the pile base should be interpolated according to Fig. 1.5 b).

For other soils (as specified in Table 1.1) values of q do not depend on the pile diameter and become constant and independent of the depth when the critical value $d_c = 10\ m$ is exceeded.

For *cohesive soils* (clays, $\varphi_u \approx 0$) the following formula may be adopted

$$q = 9 \cdot s_u$$

where s_u is undrained shear strength.

Shaft resistance

The value of the unit shaft resistance, f, is specified in Table 1.2. It depends on the type of soil and its density index I_D or liquidity index I_L.

Values of f, as shown in Table 1.2, should be used for depths equal to or exceeding 5 m below the ground level. For smaller depths the appropriate value of f ought to be determined by interpolation between the table entry and zero assumed for the initial ground level as shown in Fig. 1.6.

For *cohesive soils* (clays, $\varphi_u \approx 0$) values of f may be set depending on the undrained shear strength of soil, s_u, see Fig. 1.7.

Values of f do not depend on pile diameter.

Table 1.2. Unit shaft resistance f (kPa).

Soil type	Density index			
	$I_D = 1.00$	$I_D = 0.67$	$I_D = 0.33$	$I_D = 0.20$
Gravel, sand-gravel mix	165	110	74	59
Coarse and medium sand	132	74	47	34
Fine sand	100	62	31	22
Silty sand	75	45	25	16

	Liquidity index			
	$I_L < 0$, $w \approx 0$	$I_L = 0$, $w = w_p$	$I_L = 0.50$	$I_L = 0.75$
Loamy gravel, gravel-sand-clay mix	134	95	67	44
Loamy sand, sandy loam, loam, silty loam	95	50	31	14
Firm sandy loam, firm loam, form silty loam, sandy clay, clay, silty clay	95	59	25	11
Sandy silt, silt	65	30	16	7
Mud	48	18	0	0

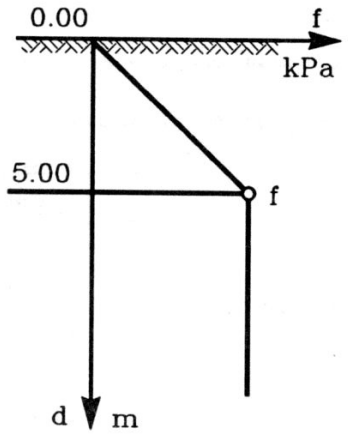

Figure 1.6: Interpolation of unit shaft resistance. Non-cohesive soils.

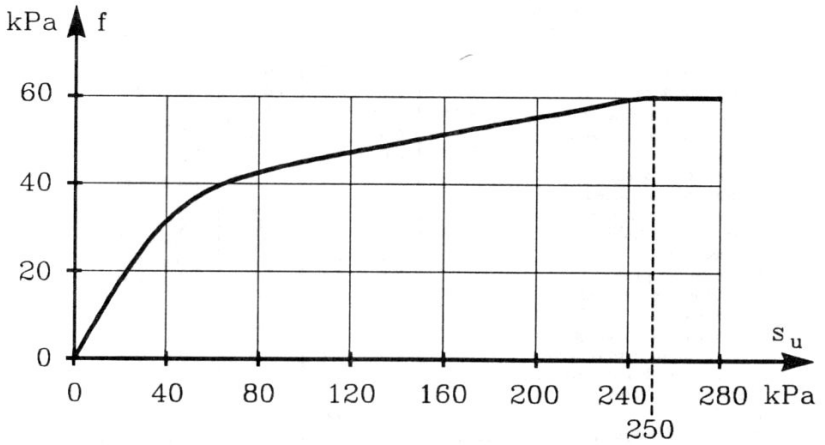

Figure 1.7: Unit shaft resistance f for cohesive soils.

Engineering factors

S_p, S_s and S^w are dimensionless factors, specified in Table 1.3.a and 1.3.b.

Table 1.3.a. Engineering factors S_p, S_s and S^w.

Ref. No.	Type of pile and method of installing	Values of the factors for soils: non-cohesive, $I_D > 0.67$: downward movement of pile S_p	$I_D > 0.67$: downward movement of pile S_S	$I_D > 0.67$: uplift of pile S^w •)	$I_D = 0.67 - 0.20$: downward movement of pile S_p	$I_D = 0.67 - 0.20$: downward movement of pile S_S	$I_D = 0.67 - 0.20$: uplift of pile S^w •)
1.	Precast reinf. concrete piles						
	a. driven	1.0	1.0	0.6	1.1	1.1	0.6
	b. installed by jetting (the last 1 m driven)	1.0	0.8	0.4	1.0	0.8	0.4
	c. driven with vibr. equip.				1.0	0.8	0.5
2.	Franki piles	1.3	1.1	1.0	1.8	1.6	1.0
3.	Vibro piles	1.1	1.0	0.6	1.4	1.1	0.6
4.	Piles bored in non-coh. soils **) (except of fine and silty sands)						
	a. in temporary casing	1.0	0.8	0.7	1.0	0.9	0.7
	b. cased	1.0	0.8	0.6	1.0	0.8	0.6
	c. with casing sunk into the ground and lifted out by means of a rotary cap	1.0	1.0	0.7	1.0	1.1	0.7
	d. in drilled fluid	1.0	1.0	0.7	1.0	1.0	0.7
	e. washbored	1.0	1.0	0.7	1.0	1.0	0.7
	f. Wolfsholz piles	1.0	0.8	0.6	1.0	0.9	0.6
5.	Piles bored in fine and silty sands **)						
	a. in temporary casing	0.8	0.8	0.4	0.9	0.7	0.5
	b. cased	0.8	0.6	0.4	0.9	0.7	0.5
	c. with casing sunk into the ground and lifted out by means of a rotary cap	0.8	0.7	0.5	0.9	0.8	0.5
	d. in drilling fluid	1.0	0.9	0.6	1.0	0.9	0.6
	e. washbored	1.0	1.0	0.7	1.0	1.0	0.7
	f. Wolfsholz piles	0.8	0.6	0.5	0.9	0.7	0.5
6.	Closed-end pipe piles						
	a. driven				1.1	1.0	0.5
	b. installed by jetting (the finale 1 m driven)	1.0	0.7	0.4	1.0	0.6	0.4
	c. driven with vibr. equipm.				1.0	0.8	0.5
7.	Steel section piles						
	a. driven	1.0	0.8	0.5	1.0	0.9	0.5
	b. installed by jetting (the final 1 m driven)	1.0	0.5	0.3	1.0	0.6	0.3
	c. driven with vibr. equipm.				1.0	0.7	0.4

•) for anchor piles used only during pile load tests values of S^w may be increased by 20%.

••) factors specified under Ref. No. 4 and 5 in the table do not cover cases of special treatment of subgrade improving its performance under the base or along the side surface. Values of the engineering factors for such cases should be based on results of site investigations.

Table 1.3.b. Engineering factors S_p, S_s and S^w.

Ref. No.	Type of pile and method of installing	Values of the factors for soils: cohesive, $I_L < 0$: downward movement of pile S_p	$I_L < 0$: downward movement of pile S_S	$I_L < 0$: uplift of pile S^w •)	$I_L = 0 - 0.75$: downward movement of pile S_p	$I_L = 0 - 0.75$: downward movement of pile S_S	$I_L = 0 - 0.75$: uplift of pile S^w •)
1.	Precast reinf. concrete piles						
	a. driven	1.0	1.0	0.7	1.0	0.9	0.6
	b. installed by jetting (the last 1 m driven)						
	c. driven with vibr. equipm.						
2.	Franki piles	1.2	1.1	0.8	1.1	1.0	0.7
3.	Vibro piles	1.0	1.0	0.6	1.0	0.9	0.6
4.	Piles bored in cohesive soils **) (except of fine and silty sands)						
	a. in temporary casing	1.0	0.9	0.6	1.0	0.9	0.6
	b. cased	1.0	0.8	0.6	1.0	0.8	0.5
	c. with casing sunk into the ground and lifted out by means of a rotary cap	1.0	1.0	0.7	1.0	1.0	0.6
	d. in drilled fluid				1.0	0.9	0.5
	e. washbored						
	f. Wolfsholz piles	1.0	0.9	0.6	1.0	0.8	0.5
5.	Piles bored in fine and silty sands **)						
	a. in temporary casing						
	b. cased						
	c. with casing sunk into the ground and lifted out by means of a rotary cap						
	d. in drilling fluid						
	e. washbored						
	f. Wolfsholz piles						
6.	Closed-end pipe piles						
	a. driven	1.0	1.0	0.5	1.0	0.9	0.5
	b. installed by jetting (the finale 1 m driven)						
	c. driven with vibr. equipm.						
7.	Steel section piles						
	a. driven	1.0	1.0	0.5	1.0	0.9	0.5
	b. installed by jetting (the final 1 m driven)						
	c. driven with vibr. equipm.						

•) for anchor piles used only during pile load tests values of S^w may be increased by 20%.

••) factors specified under Ref. No. 4 and 5 in the table do not cover cases of special treatment of subgrade improving its performance under the base or along the side surface. Values of the engineering factors for such cases should be based on results of site investigations.

Open ended piles

The open ended pipe piles should be determined according to formula:

i) in compression

$$Q = Q'_p + Q'_s = b_1 \cdot q \cdot A_p + \sum b_2 \cdot S_{si} \cdot f_i \cdot A_{mi}$$

ii) in uplift

$$Q^t = \sum b_2 \cdot S_i^w \cdot f_i \cdot A_{mi}$$

where b_1 and b_2 are reduction factors as specified in Table 1.4 and Table 1.5.

In the case of non-cohesive soils of large grain size and higher degree of compaction, the actual bearing capacity of a pile will be larger than that calculated based on these values.

Use of open ended pipe piles in non-cohesive soils characterized by degree of compaction lower than 0.4 is not recommended.

Table 1.4. Values of b_1 and b_2 for non-cohesive soils.

No.	$I_D = 0.40$				$I_D = 0.70$			
	d/D		b_1	b_2	d/D		b_1	b_2
	moist	wet			moist	wet		
1					4.0	6.0	0.22	0.27
2	6.0	9.0	0.28	0.61	5.5	8.0	0.50	0.35
3	7.5	11.5	0.78	0.61	6.5	10.0	0.90	0.37
4	17.0	26.0	1.00	0.61	17.0	26.0	1.00	0.65

Table 1.5. Values of b_1 and b_2 for cohesive soils.

No.	d/D	Liquidity index $I_L \leq 0.50$ and $f \geq 20\ kPa$		
		b_1	b_2	
			steel pipe	reinforced concrete pipe
1	6 - 15	0.7	0.8	1.0
2	15	pipe empty inside = 0.9	0.8	1.0
		pipe filled with concrete = 1.0		

Notes to tables of b_1 and b_2

i) the small relative penetration depths d/D specified in the tables should be regarded as minimum required for driven open ended pipe piles.

ii) the factors b_1 and b_2 for intermediate values of relative penetration depths and for $0.4 < I_D < 0.7$ ought to be determined by linear interpolation. For $I_D \geq 0.7$, b_1 and b_2 is assumed to be constant.

Chapter 2

Penetrometer tests

The development of oil and gas fields in the North Sea with new platform concepts lead to very advanced soil investigations in terms of sampling and especially in site testing (T. Lunne, S. Lacasse, 1987). The cone penetration test (CPT) has been the dominant in site tool. Now several other tools have been developed for offshore investigation: piezocone (CPTU), vane shear test (VST), pressuremeter test (PT), and dilatometer test (DMT).

The first soil investigations in the North Sea were performed in 1965/66 as simple soil borings. Cone penetration testing was first performed in 1972 and is now a routine part of detailed site investigation.

For offshore investigation equipment has been developed that can be placed on the seabed. The penetration depth depends very much on the soil conditions. In the hard soils 8 to 15 m penetration can be reached and in the soft soils about 30 meters.

The electrical cone has been standardized (ISMFE, 1977 and ASTM, 1979), Fig. 2.1:

- cone with an apex angle 60° and base area of 10 cm^2
- friction sleeve located immediately behind the cone having an area of 150 cm^2
- speed of pushing cuts the ground of 2 cm/sec.

The piezocone, Fig. 2.1 and 2.2, consists of a standard electrical cone

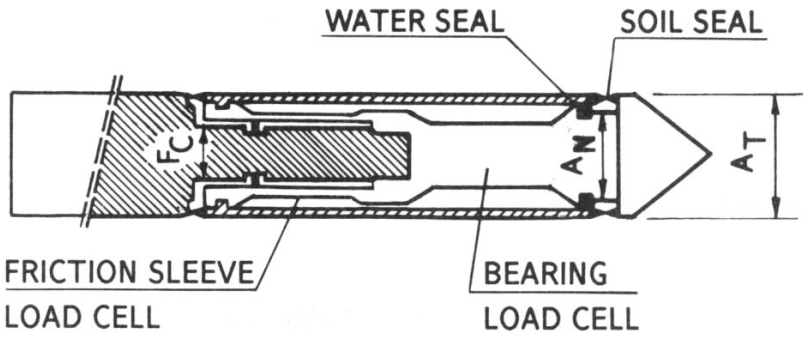

Figure 2.1: Typical electric cone (Schaap and Zuidberg, 1982).

penetrometer which is provided with a filter (porous stone) at the tip and a pressure transducer. The pore water pressure of the tip can be recorded with cone resistance and sleeve friction.

2.1 Undrained shear strength

The undrained shear strength, s_u, was obtained from

$$s_u = \frac{q_c - \sigma_{vo}}{N_k} \tag{2.1}$$

where q_c cone resistance measured
σ_{vo} in situ total overburden stress
N_k empirical cone factor related to q_c, see Fig. 2.3 and 2.6,
recommended values between 15 and 20.

(Aas, G. et al., 1987)

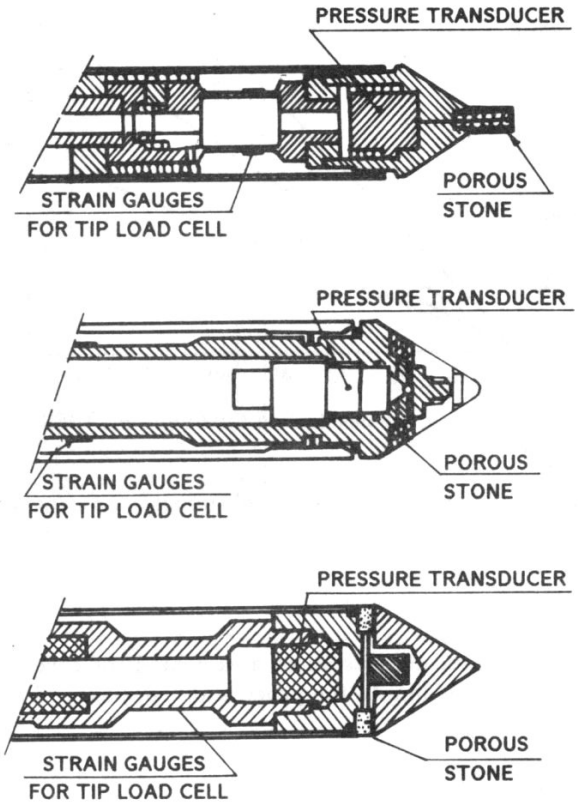

Figure 2.2: Example of existing piezocones (Jamiolkowski, 1985).

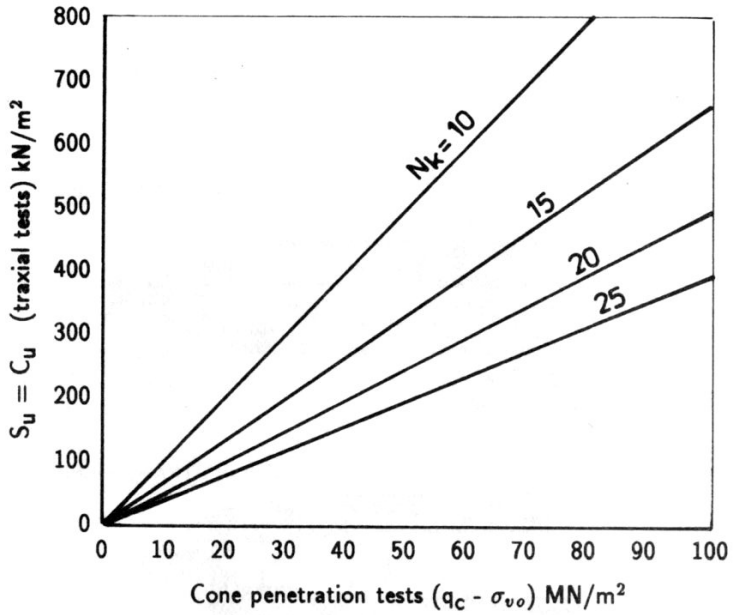

Figure 2.3: Relation between undrained strengths measured in triaxial tests and the net cone resistance for North Sea clays (after Kjekstad et al., 1978).

Since water pressure acts on an area behind the cone, the cone resistance, q_T, corresponding to the penetration resistance of a jointless cone is:

$$q_T = q_c + u(1 - a) \tag{2.2}$$

where u pore pressure behind cone during penetration
a area ratio (constant for a specific cone), see Fig. 2.4 and Fig. 2.5.

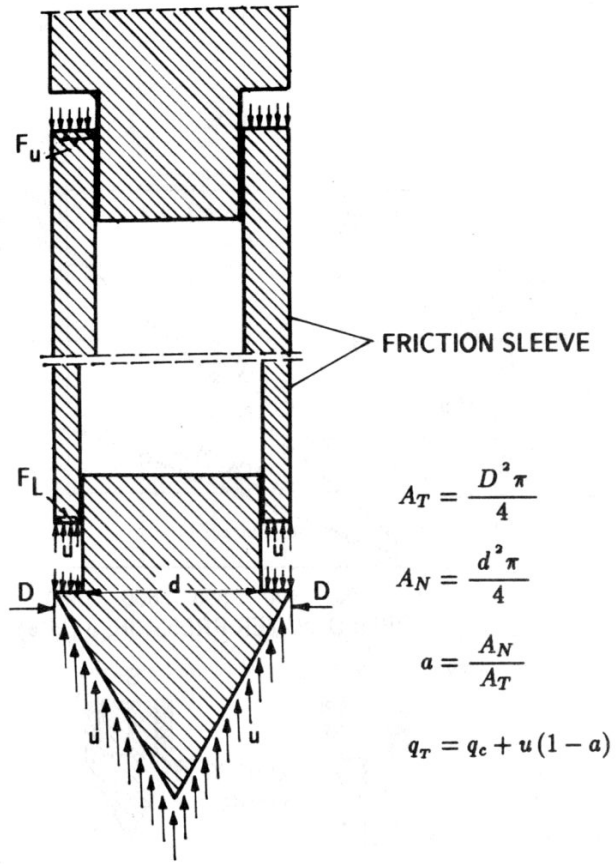

Figure 2.4: Unequal end areas of the electrical friction cone (Jamiolkowski, 1985).

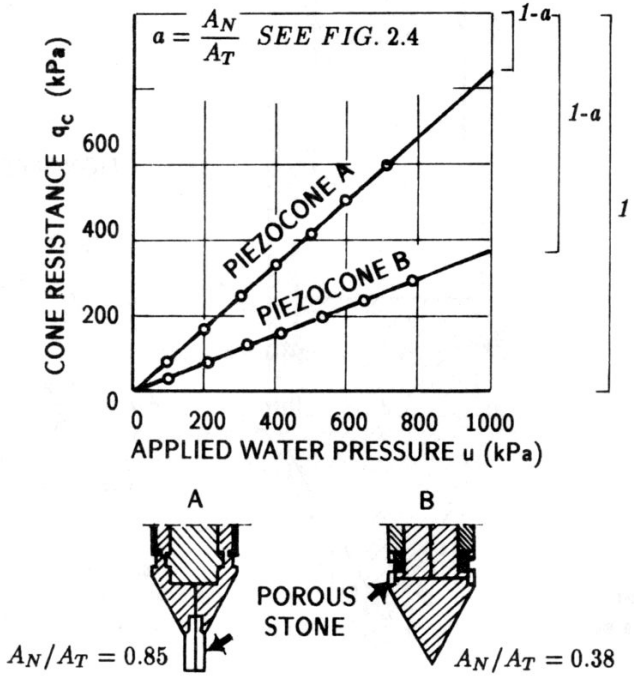

Figure 2.5: An example of determination of A_N/A_T in the pressure chamber (Battaglio and Maniscalco, 1983).

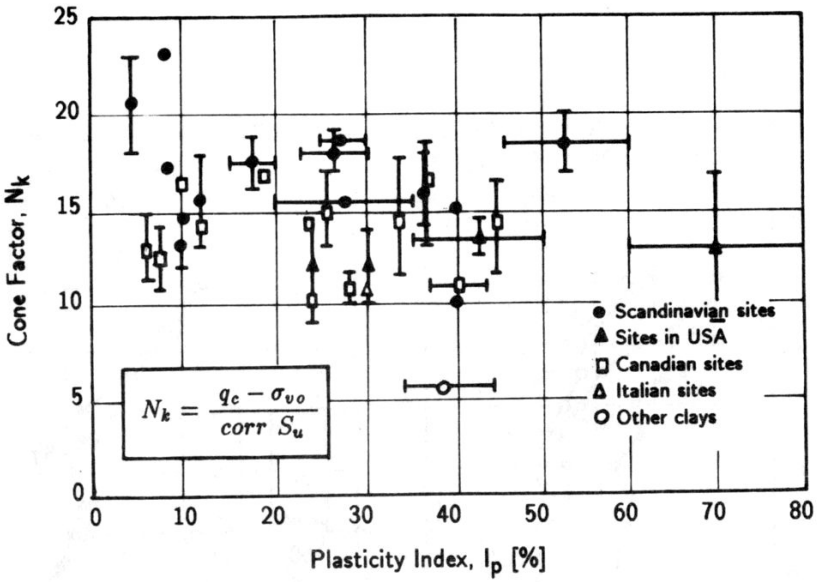

Figure 2.6: Example of $N_k - I_p$ correlation as proposed by different workers. Data are inconsistent since the different cones used had different area ratios (Aas, G. et al., 1987).

The undrained shear strength related to the failure caused by cone penetration is then:

$$s_u = \frac{q_T - \sigma_{vo}}{N_{kT}} \tag{2.3}$$

where N_{kT} is the empirical cone factor related to q_T, see Fig. 2.6, according to Baligh et al. (1980), Lunne and Kleven (1981), Azzouz (1985), Baligh (1985).

Fig. 2.7 shows profiles with two different piezocones in the Norwegian Emmerstad quick clay ($I_p = 3 - 10\%$), as an example.

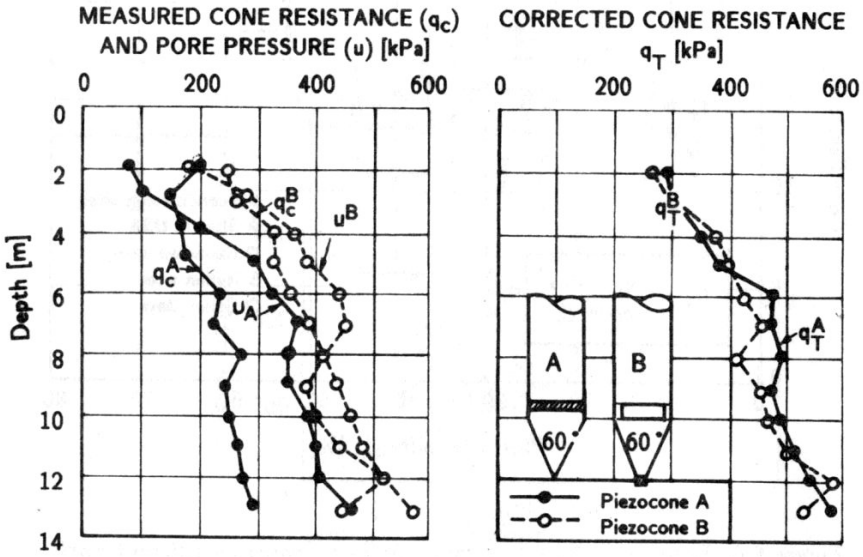

Figure 2.7: Effect of pore pressure on cone resistance in Emmerstad quick clay (Aas, G. et al., 1987).

2.2 Soil identification

Use of penetrometer permits a continuous measurement of both the cone resistance q_c and local shaft friction f_s. The ratio of the sleeve friction f_s and cone resistance q_c enables identification of the soil type (Begemann, 1965; Sanglerat, 1972; Schmertmann, 1975; De Ruiter, 1987; Robertson and Campanella, 1984), see Fig. 2.8 and 2.9.

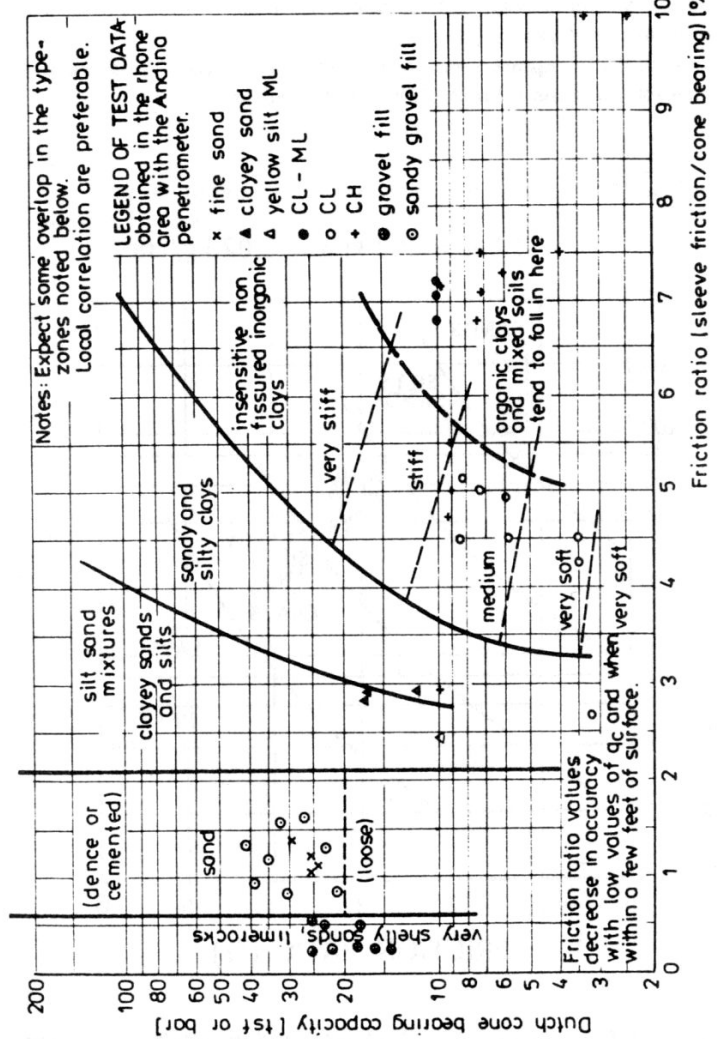

Figure 2.8: Soil classification from q_c and the ratio $FR = f_s/q_c$. Correlation between Schmeltmann's soil classification curves and tests performed in France with the Andina penetrometer (Sanglerat, 1972).

The friction as percentage of the cone resistance is high in clay and low in coarse sand and gravel.

Piezocone (CPTU) appears to be a good tool for soil identification. The best theoretical basis (Wroth, 1984) is defined as:

$$B_q = \frac{u - u_o}{q_T - \sigma_{vo}} \tag{2.4}$$

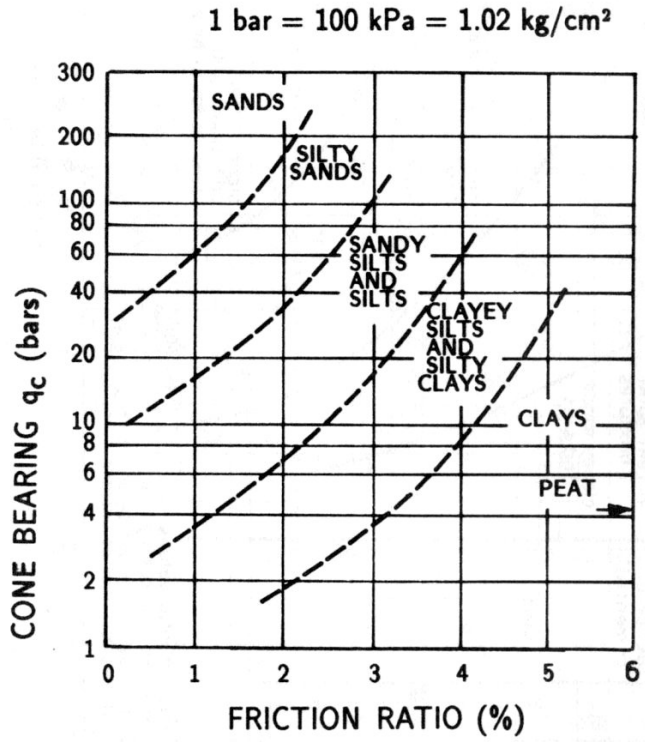

Figure 2.9: Simplified classification chart for standard electrical friction cone (Robertson and Campanella, 1984).

where B_q — CPTU pore pressure coefficient
u — penetration pore pressure
u_o — hydrostatic pore pressure
σ_{vo} — total overburden stress
q_T — total cone resistance corrected for the unequal end area effect

Using the parameter B_q Senneset and Janbu (1984) presented the tentative soil classification, Fig. 2.10.

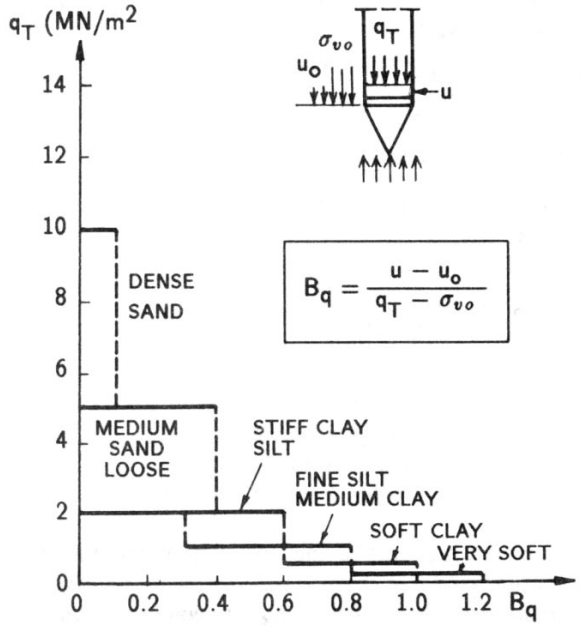

Figure 2.10: Tentative classification chart based on q_c and B_q for standard electrical friction cone (adapted from Senneset and Janbu, 1984).

2.3 Drained shear strength

A number of methods exist for interpretation of cone resistance in terms of drained shear strength. Most of those methods are based on bearing capacity theory which assumes slip failure (classical bearing capacity) worked out for plain strain conditions and modified for circular foundations. Recent theories are based on cavity expansion theory. The NGI study selected four methods to compute drained shear strength from the cone data base and to compare with results of triaxial tests. The four methods are: Meyerhof (1961), Durgunologu and Mitchell (1975), Janbu and Senneset (1975), Schmertmann (1978).

1. Meyerhof (1961) proposed the relationship between φ' and N_q as shown in Fig. 2.11, where

$$N_q = \frac{q_c}{\sigma'_v} = \frac{q_c}{\gamma' \cdot z} \tag{2.5}$$

and γ' is the effective soil unit weight.

2. Durgunologu and Mitchell (1975) developed a theory based on a general shear failure.
For cohesionless soils the theory leads to:

$$q_c = \gamma' \cdot B \cdot N_{\gamma q} \cdot \xi_{\gamma q} \tag{2.6}$$

where B — cone diameter
$N_{\gamma q}$ — bearing capacity factor for wedge penetration
$\xi_{\gamma q}$ — shape factor to convert wedge factors to cone factors

The product $N_{\gamma q}, \xi_{\gamma_q}$ can be considered as a cone factor dependent on soil friction angle φ', base roughness δ/φ', relative depth d/B, lateral earth pressures coefficient K_o and cone apex angle. For $K_o = 0.4$ and $K_o = 1.0$, depth 10 m and $\gamma' = 10\ kN/m^3$ the values are given in Fig. 2.11.

3. Janbu and Senneset (1975)
The cone resistance is:

$$q_c + a = N_q(\sigma'_v + a) \tag{2.7}$$

or

$$q_p = N_p(\sigma'_v + a) \tag{2.8}$$

where a — "attraction", $a = c' ctg\varphi'$
typically $a = 0 - 50kPa$ for sand
$N_p = N_q - 1$
$q_p = q_c - \sigma'_v$
N_q — bearing capacity factor, depends on the angle of plasticification β, see Fig. 2.11.

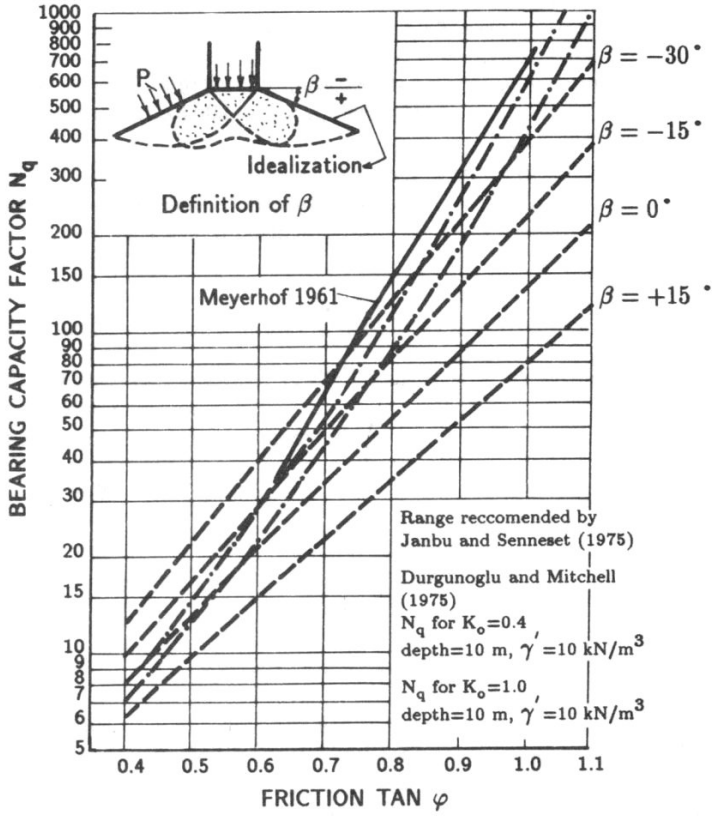

Figure 2.11: Bearing capacity factors from various theories.

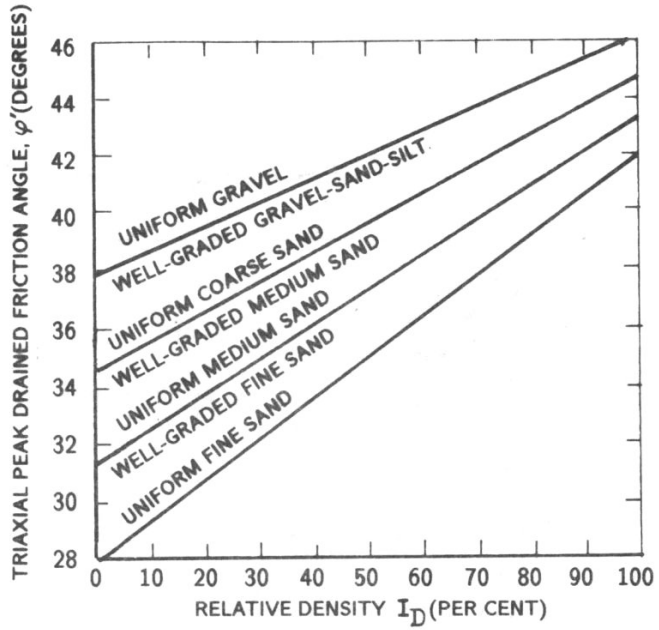

Figure 2.12: Relationship between φ' and I_D, suggested by Schmertmann, 1978.

4. Modified Schertmann method

To estimate the friction angle φ', Schmertmann (1976 and 1978) recommended an interest method based on the relative density I_D, Fig. 2.12. Based on a recently available calibration chamber test results, Lunne and Christoffersen (1983) suggested revised I_D, q_c, σ'_{vo} correlation as shown in Fig. 2.13. Fig. 2.14 reports the correlation between I_D and go through σ'_{vo} worked out by Lancellotta (1983) as well.

Recommendations

For normally consolidated or slightly overconsolidated sands

(i) Use the Durgunologu and Mitchell's method with $K_o = 0.4$.

(ii) Use the modified Schmertmann method, see Fig. 2.13 and Fig. 1.12.

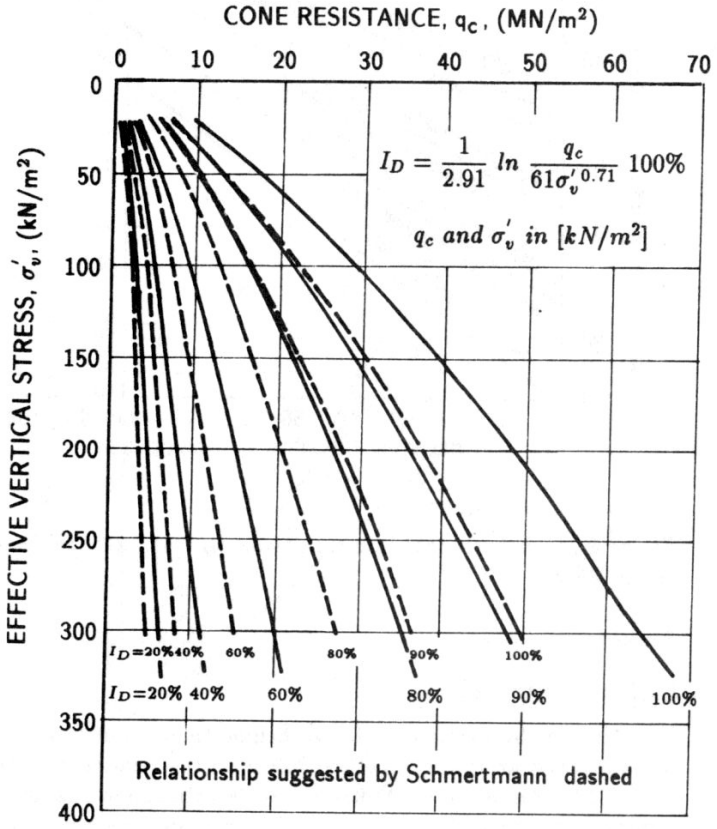

Figure 2.13: Recommended relationship among σ'_v, q_c and I_D, for NC fine-medium quartz sand (Lunne and Christoffersen, 1983, 1985).

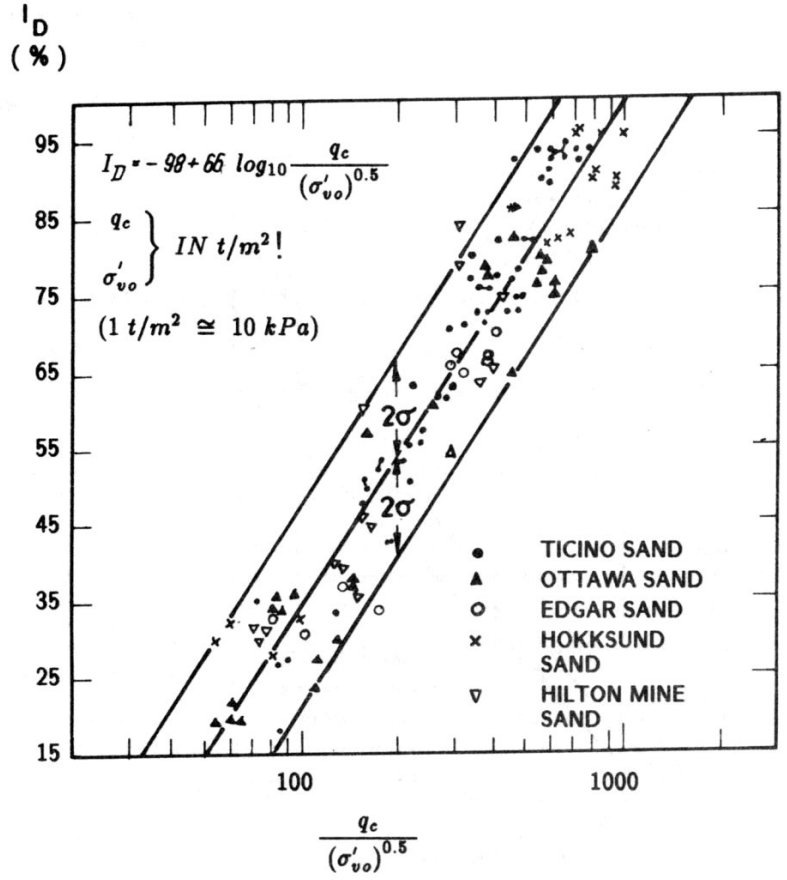

Figure 2.14: Correlation between I_D and q_c through σ'_{vo} (Lancellotta, 1983).

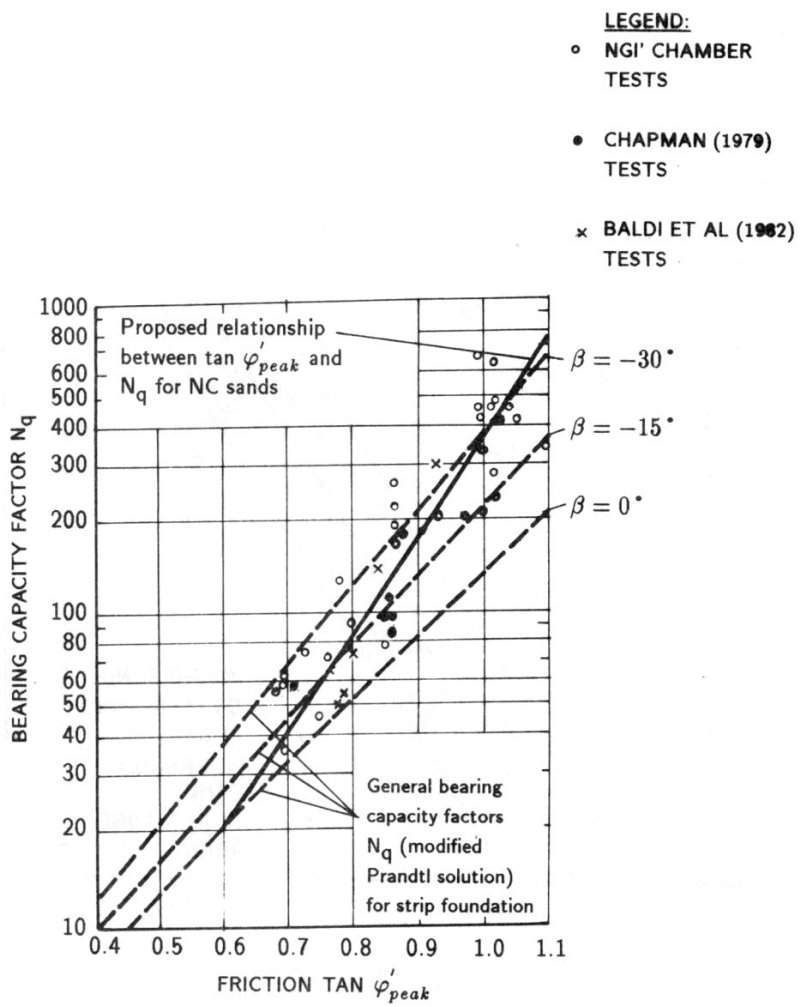

Figure 2.15: Bearing capacity factor N_q versus $tan\varphi'_{peak}$ from tests on NC sands (Janbu, Senneset, 1975, Lunne, Christoffersen, 1985).

(iii) Use a modified Janbu and Senneset method, see Fig. 2.15, with

$$N_q = tan^2(45° + \varphi'/2)\, e^{\left(\frac{\pi}{3}+4\varphi'\right)\cdot tan\varphi'} \tag{2.9}$$

and, taking into account relationship (2.5).

For overconsolidated sands, OCR and K_o should be estimated and q_{coc} (overconsolidated) should be recalculated to q_{cnc} (normally consolidated), as below:

$$\frac{q_{coc}}{q_{cnc}} = 1 + 0.75\left(\frac{K_{ooc}}{K_{onc}} - 1\right) \tag{2.10}$$

where $\frac{K_{ooc}}{K_{onc}} = (OCR)^{\beta_1}$, it is recommended to use $\beta_1 = 0.45$.

2.4 Deformation characteristics

Three different moduli are used in practice:

1. Constrained modulus, M, for one-dimensional loading, corresponding to oedometer testing.
2. Young's modulus, E, for non-one-dimensional cases (equivalent to the modulus from triaxial tests).
3. The initial shear modulus G (used in calculations of dynamics response and for the load displacement relationship at the pile shaft, for example).

The following important points should be kept in mind in the practice (Jamiolkowski et al., 1985):

1. Each of the soil deformation parameters depends on the octahedral effective stress, σ'_{oct} and the stress history, i.e.:

$$E \text{ or } G \text{ or } M = f(\sigma'_{oct}, OCR) \tag{2.11}$$

2. Both E and G are strongly dependent on the in situ shear stress level.
3. The drainage conditions should be taken into account.
4. The deformation moduli obtained from in situ tests reflect both the degree of anisotropy of the soil and the stress path followed.

Constrained modulus M

The initial tangent constrained modulus, M_o, and secant modulus, M, are defined by:

$$M_o = \frac{d\sigma'_v}{d\varepsilon} \quad , \quad \text{taken at} \quad \sigma'_{vo} \tag{2.12}$$

where σ'_{vo} is the initial effective vertical stress

$$M = \frac{\Delta\sigma'_v}{\Delta\varepsilon_v} \quad , \quad \text{between} \quad \sigma'_{vo} \text{ and } \sigma'_{vo} + \Delta\sigma'_v \tag{2.13}$$

According to NGI review, a conservative initial tangent modulus, M_o, in normally consolidated sands can be computed as follows, see Fig. 2.16:

$$M_o = 4 \cdot q_c \quad \text{for} \quad q_c < 10\ MPa \tag{2.14}$$

$$M_o = (2q_c + 20\ MPa) \quad \text{for} \quad 10\ MPa < q_c < 50\ MPa \tag{2.15}$$

$$M_o = 120\ MPa \quad \text{for} \quad q_c > 50\ MPa \tag{2.16}$$

For sands with $OCR > 2$, M_o-values can be used:

$$M_o = 5q_c \quad \text{for} \quad q_c < 50\ MPa \tag{2.17}$$

$$M_o = 250q_c \quad \text{for} \quad q_c > 50\ MPa \tag{2.18}$$

The constrained modulus applicable for the stress range σ'_{vo} to $\sigma'_{vo} + \Delta\sigma'_v$ can be estimated as:

$$M = M_o \sqrt{\frac{\sigma'_{vo} + \frac{\Delta\sigma'_v}{2}}{\sigma'_{vo}}} \tag{2.19}$$

Experience has shown that for many normally consolidated sands the modulus M can be expressed as:

$$M = m \cdot p_a \sqrt{\frac{\sigma'_v}{p_a}} \tag{2.20}$$

where σ'_v — average effective vertical stress
p_a — reference stress, $p_a = 100kPa$
m — factor depending on the density of sand.

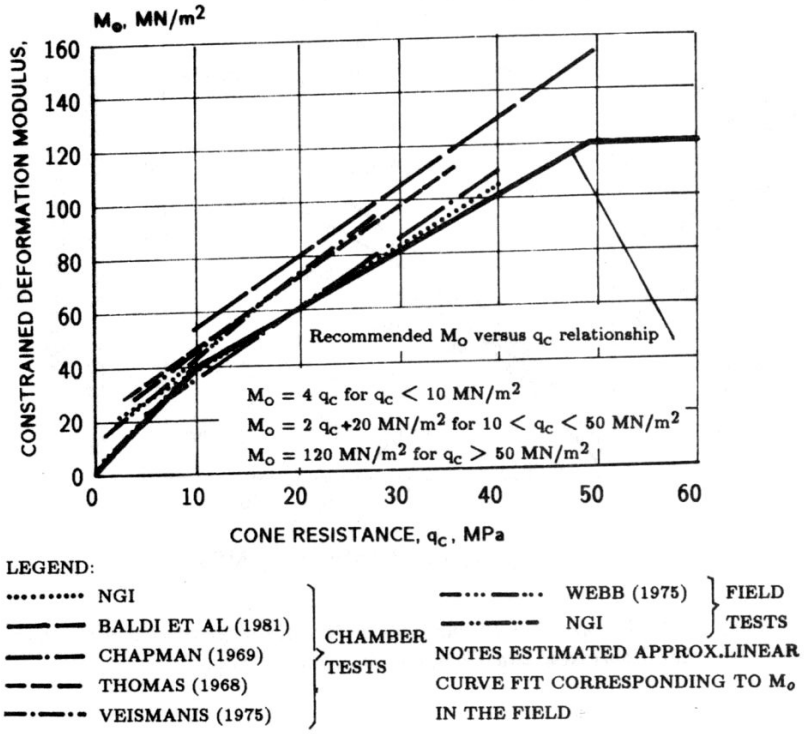

Figure 2.16: Summary of relationships between constrained modulus M_o and cone resistance q_c for NC sands (Lunne and Christoffersen, 1985).

Young's modulus, E

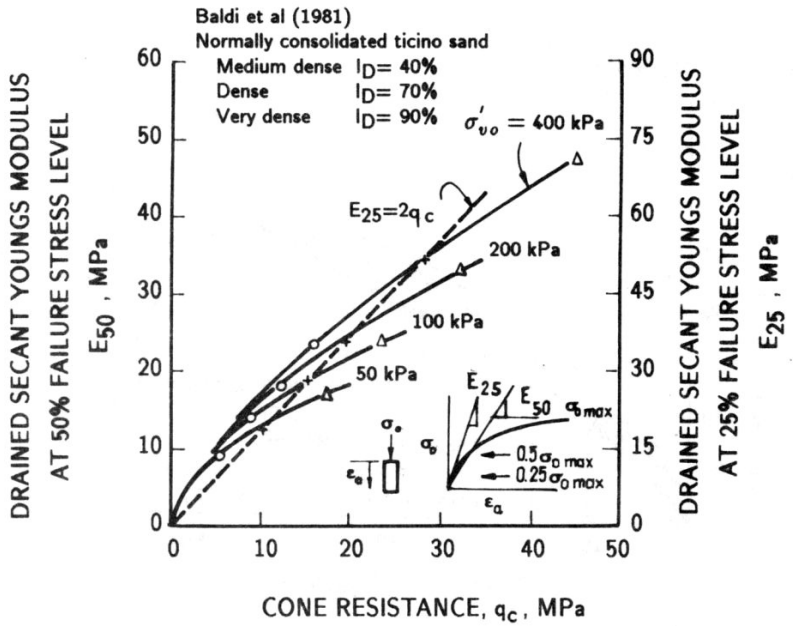

Figure 2.17: Secant Young's modulus values for uncemented n.c. quarts sands (after Robertson and Campenalla, 1983).

Robertson and Campanella (1983) reviewed calibration chamber test results where cone resistance was compared to drained secant modulus from parallel triaxial tests and presented the recommendation given in Fig. 2.17. Robertson and Campanella (1983) argued that E_{25} (secant modulus at 25% failure shear stress) is the most appropriate since the safety factor against bearing capacity failure is usually around 4 for foundations on sand. For computing the bearing capacity of piles E_{50} may be more adequate.

Initial shear modulus

The chart in Fig. 2.18 gives prediction of G_{max} for normally consolidated, fine to medium uniform non-cemented sands (Robertson and Campanella, 1983).

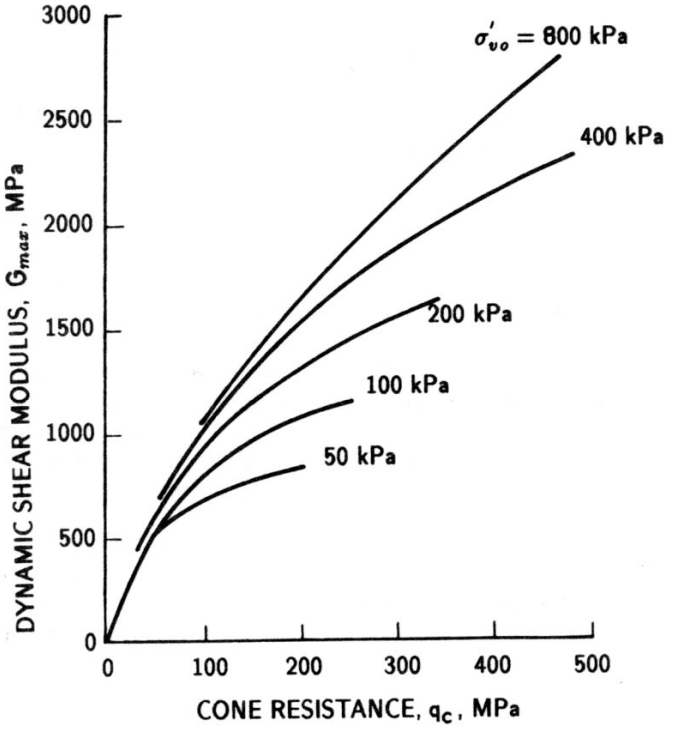

Figure 2.18: Dynamic shear modulus values for uncemented n.c. quartz sands (after Robertson and Campanella, 1983).

Chapter 3

Installation of offshore piles

Piles may be classified by:
Materials: concrete, reinforced concrete, wood and steel.
Installation procedures: driven, cast-in-place, jacked, screw piles.
Function: friction piles, end bearing piles.
Volume mass displacement around the pile:

- — displacement piles (prefabricated concrete, timber, close-ended steel piles.
- — small displacement piles (H-piles, open ended pipe piles).
- — non-displacement piles (bored piles, drilled caissons).

The procedures for installation of offshore piles are in many ways different from installation procedures on land. In this chapter some aspects of pile installation offshore are presented, according to McClelland, Focht and Emrich (1969).

3.1 Installation by pile hammers

The pile installations of offshore foundations can be done using pile driving alone (Fig. 3.1). Some of these installations are fully successful because soil resistance during driving is low in comparison to hammer capability.

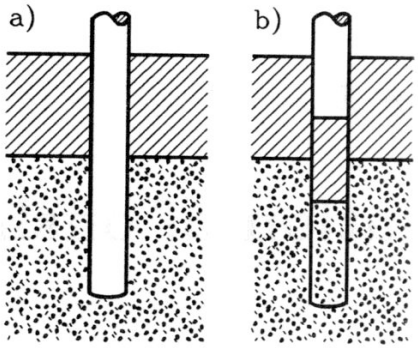

Figure 3.1: Driving piles,
a) close ended steel piles, b) open ended pipe piles.

3.2 Installing undrivable piles

When capacity of hammers aren't big enough to drive piles into suitable level, methods supplemental to driving must be employed.

Supplemental installation methods may be divided into four categories:

(i) Driving an insert pile through an initially installed larger pile.
(ii) Grouting a pile into an oversized hole.
(iii) Driving a pile concentrically with an undersized pilot hole.
(iv) Driving a pile with the aid of uncontrolled drilling or jetting.

3.2.1 Insert pile

An insert pile is driven trough and penetrates below the tip of a previously installed larger diameter pile, see Fig. 3.2 a). Very often the upper end of

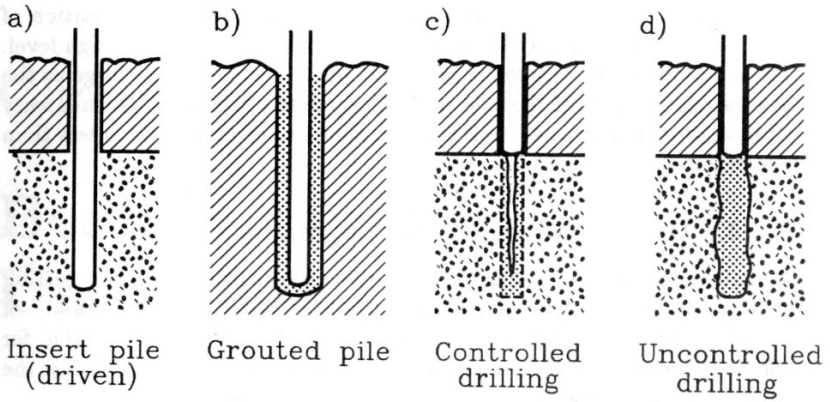

Figure 3.2: Installation procedures currently in use for piles that cannot be installed by driving alone.

the insert pile is welded to the initial pile.

3.2.2 Grouted piles

The installation procedure of a grouted pile includes, see Fig. 3.2 b):

— drilling of an oversized hole up to end of the design pile
— placing the pile in the centre of the drilled hole
— grouting the space between the wall (shaft) of the pile and surrounding soil

Grouting requires the use of large-hole drilling techniques.

3.2.3 Controlled pilot hole

Another supplemental method to drive the pile is to drill a pilot hole of controlled dimensions through the pile, to some depth below the pile tip, and then to redrive the pal, see Fig. 3.2 c). More than one repetition of the drilling – driving may be required before the pile reaches design level. The cross-sectional area of the pilot hole should be at least as large as the cross-sectional area of the pile wall. The range of the pilot holes is very often approximately one – half the pile diameter to about 10 cm less than pile diameter.

3.2.4 Uncontrolled drilling or jetting

A common method of installation of driven piles is the drilling or jetting of a controlled hole, see Fig. 3.2 d), either internally or externally of the pile. This technique of pile driving is rather seldom acceptable for offshore structures. It is impossible to predict with good accuracy the bearing capacity of a pile installed with uncontrolled drilling.

Chapter 4

Bearing capacity. Undrained case

The ultimate bearing capacity of a single pile Q consists of point resistance Q_p and shaft resistance Q_m:

$$Q = Q_p + Q_m \tag{4.1}$$

In clay Q_p is normally much lesser than Q_m. Q_p can therefore be determined by a rather rough assumption, but Q_m must be handled with care.

4.1 Point resistance Q_p

The estimation of Q_p is most simply considered as a bearing capacity problem:

$$q_p = Q_p/A_p = s_u \; N_c^\circ \; s_c \; d_c + q_v \tag{4.2}$$

where $N_c^\circ = \pi + 2$, as usual, $s_c = 1.2$ for circular and squared piles and the depth factor is $d_c \approx 1.35$ for $d/D > 1$, as proposed by Brinch Hansen. The total overburden pressure q_v at tip level is assumed to balance the

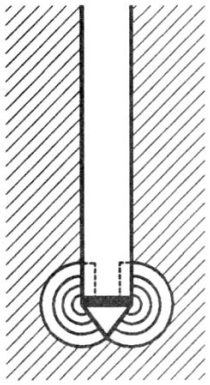

Figure 4.1: Kinematically admissible solution for a footing in a deep excavation.

Since a depth factor is used the formulas require that the soil moves from the pile tip to the ground surface, and this is obviously not the case.

Fig. 4.1 shows a kinematically admissible solution, which in the plane state gives

$$q_p = 8.9\ s_u \tag{4.4}$$

corresponding to a depth factor of $d_c = 1.73$. When the footing is pressed down into the soil, which has a constant volume, the clay has to move into the deep excavation.

If a pile is installed in the excavation the volume of the clay must be pressed out into the surrounding soil, and an additional total pressure grows up, and the tip resistance increases.

The combined effect of the usual bearing capacity problem and the elastic volume displacement can be taken into account by introducing a stiffness factor r_c:

$$q_p \approx 9\ s_u \cdot r_c \tag{4.5}$$

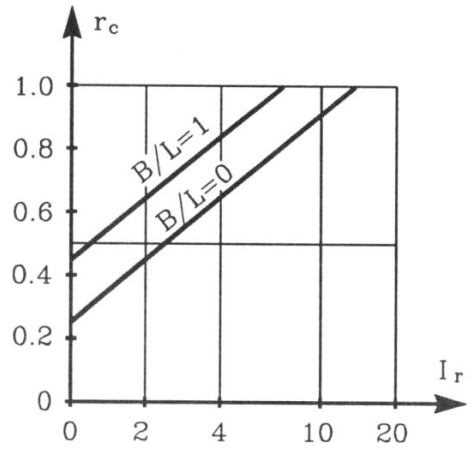

Figure 4.2: Stiffness factor r_c.

as proposed by Kulhawy (1984). Vesic (1975) calculated the values of r_c, shown in Fig. 4.2.

I_r is the so-called rigidity index, defined as:

$$I_r = \frac{G}{c + q\ \tan\varphi}$$

corresponding to depth at half the pile length. Vesic's theory gives values of r_c lesser than 1, which is astonishing. But it seems reasonable that r_c in stiff clay is twice the r_c in soft clay. [1]

The point resistance depends also on the roughness of the pile shaft near the end of the pile. Formulas (4.3) and (4.5) are based on a smooth pile shaft.

4.2 Shaft resistance

Calculation of Q_m is based on a great number of pile loading tests, performed on different piles in different soils and with different installation

[1] Compare DS 415: In stiff moraine clay $q_p = 18\ c_u$.

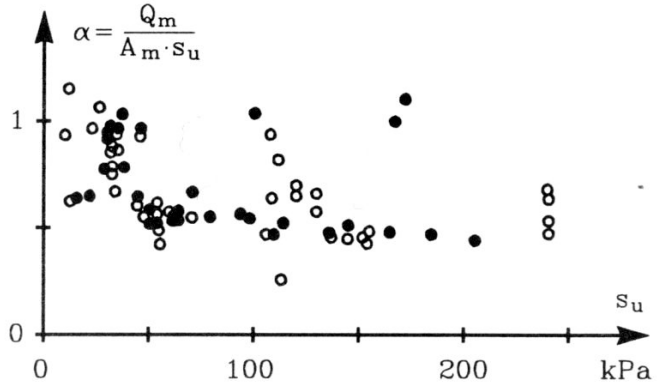

Figure 4.3: Test results reduced by Q_p.
• *API (Semple and Rigden)* o *Vijayvergiya and Focht.*

methods. In pile loading tests the total capacity of the pile Q is measured. Q_m is then determined by reducing Q with the rough calculated resistance Q_p, and this causes some of the scatter in the "test results" (see Fig. 4.3).

According to Fig. 4.3 the shaft resistance may be expressed as

$$f = Q_m/A_m = \alpha s_u \tag{4.6}$$

This method is called the α-method.

Several authors have developed formulas or curves for the variation of α with s_u. (Kerisel (1961), Peck (1953), Tomlinson (1957), Woodward (1961)). There are big differences between the α-values corresponding to the same s_u-value, but different authors, because they referred to different tests.

Many codes are based on pile tests referred to in Fig. 4.3 or special national pile test series (Fig. 4.4). Of special interest is the API-code (American Petroleum Institute) since it is widely used.

By comparing Fig. 4.4 and 4.3 it is seen that the codes are in reasonable agreement with the pile loading tests, but it is obvious too that some more factors should be included.

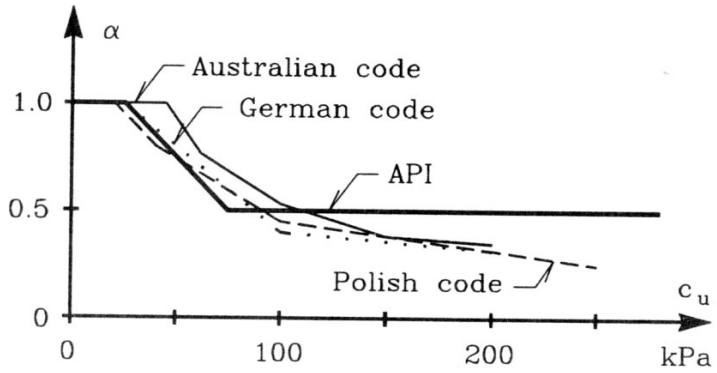

Figure 4.4: α-values from different codes.

i) Surface of pile.

Reese and O'Neill (1972) proposed a surface factor β_1, which should be 1 for a pile installed in dry hole, but only 0.6 if drilling with slurry.

Broms (1978) and the Swedish Code (SB 14, 1975) suggest that in soft clays the surface roughness plays a role:

$\alpha = 0.8$ for concrete piles
$\alpha = 0.5$ for steel piles

ii) Preconsolidation pressure.

Many authors have noted that α depends on the overconsolidation ratio OCR , Wroth (1972), McLelland (1974), Randolph and Wroth (1982), Semple and Rigden (1984).

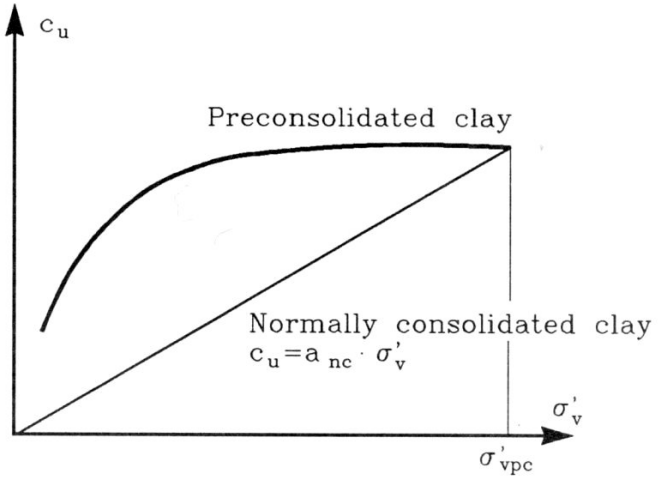

Figure 4.5: s_u depends on the effective overburden pressure.

OCR is difficult to calculate, because the preconsolidation pressure should be estimated from laboratory tests first. Fig. 4.5 shows that it should be possible to use s_u/σ'_v instead, and this quantity can be deduced directly from site investigation data. There is still a possibility of getting some scatter in the test results since a_{nc} is not a constant, but depends on the type of clay. Semple and Rigden's results are shown in Fig. 4.7, where their proposal for α-values for $L/D > 60$ is shown too.

iii) Length of pile.

Fig. 4.6 indicates that when the pile length increases the α_{OCR}-value will be reduced. If the pile is long and elastic, it is possible that the adhesion at small depth may be reduced to its residual value, see part 7.), even before the total maximum shaft adhesion is mobilized. The α-value can then be calculated by

$$\alpha_L = \alpha_{OCR} \cdot LF$$

where LF is shown in Fig. 4.7. The OCR-method gives a rather close agreement between the calculated and observed values.

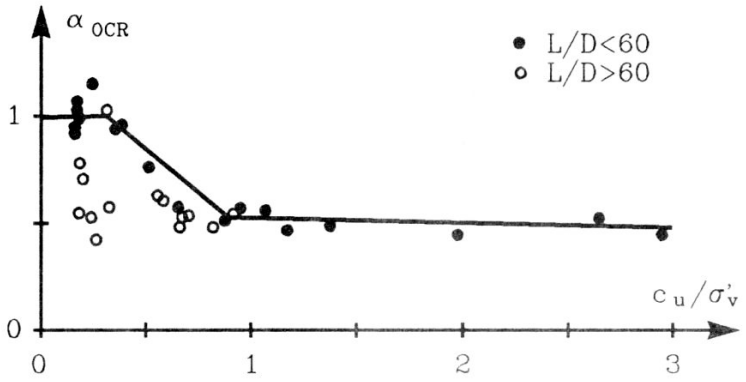

Figure 4.6: α versus strength ratio.

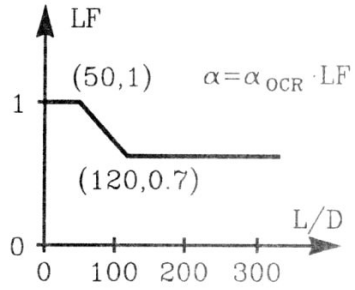

Figure 4.7: Influence of pile length (Semple and Rigden 1984).

Other authors, who do not take the preconsolidation pressure into account and use results from Fig. 4.3, find that the long piles have bigger α-values than the short ones.

Reese and O'Neill (1972) proposed

$$LF = (1 - 2.5/D)^2 \qquad \text{with } D \text{ in feet (!)}$$

4.2.1 Experimental determination of α

The mentioned α-values are determined from pile loading tests, where the ultimate load has been reduced by a calculated point resistance. It is a very expensive way to get an idea of the size of α, and it is possible to make many mistakes.

So — it seems reasonable to make laboratory tests – even in small scale — and compare these results with the back-calculated ones. At AUC some small scale tests have been carried out by students and by K. Gwizdala. The main results are shown in Table 4.1 and Table 6.2 and agree well with values from the literature.

Table 4.1. AUC test results.

Type of piles	Clay		Sandy clay	
	s_u (kPa)	α	s_u (kPa)	α
Smooth, installed pile	50 - 160	0.24 - 0.35	60 - 240	0.22 - 0.13
Rough, installed pile	55 - 160	0.40 - 0.53	80 - 240	0.46 - 0.35
Smooth, driven pile			40 - 180	0.24 - 0.41
Rough, driven pile			40 - 190	0.65 - 0.39
Smooth, pushed pile			80 - 160	0.35 - 0.41

The values of α depends on roughness and technology of the piles and type of the soil, see in Fig. 4.8.

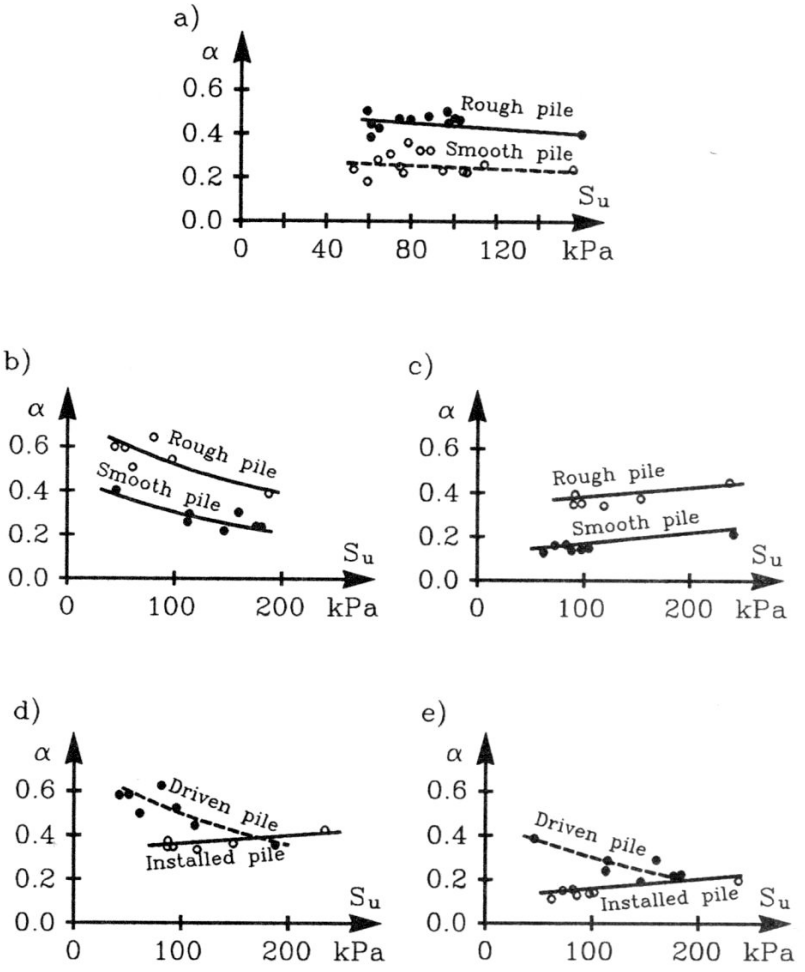

Figure 4.8: The values of the parameter α according to AUC test results. a) Installed piles in clay. b) Driven piles in moraine clay. c) Installed piles in moraine clay. d) Rough piles in moraine clay. e) Smooth piles in moraine clay.

Technology of piles during model tests:
- installed, piles placed in the box before soil consolidation
- driven, piles are driven into the box with hammer after consolidation.

It is seen by comparing Fig. 4.4 and 4.6 that the codes are in reasonable agreement with the test results.

Chapter 5

Bearing capacity. Drained case

The ultimate bearing capacity of a single pile in sand or under drained conditions in clay must be estimated from effective stresses and effective soil parameters.

When piles are driven into sand, the soil close to the pile is compacted. When piles are driven into clay, the clay is first remoulded, and then during consolidation compacted. So it is rather difficult to find a correlation between the in situ soil parameters and the bearing capacity of a pile.

Large scale experiments and field observations show, however, that a theoretical relationship holds when the pile tip is above a certain depth, called the critical depth, d_c. At greater depth the point resistance and the average shaft resistance as well can be taken as a constant.

The critical depth for driven piles is shown in Fig. 5.1. It depends on the effective friction of the soil. For bored piles the critical depth may be increased by 20-40%.

When piles penetrate through a weak stratum into a thick layer of firm soil, the bearing capacity in the weak soil follows the above mentioned rules. When the pile tip penetrates into the dense soil the bearing capacity grows up. When the penetration depth exceeds 10D the point resistance in the dense sand is fully developed [1]. According Meyerhof (1976) d_c should

[1] Normal Danish practice: 5D

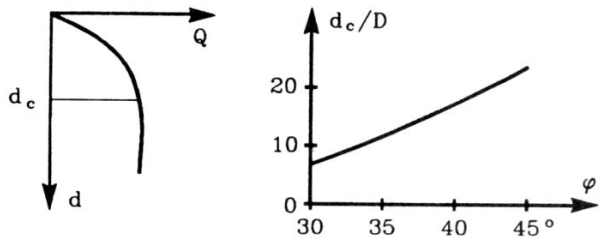

Figure 5.1: Critical Depth Ratio for Driven Piles.

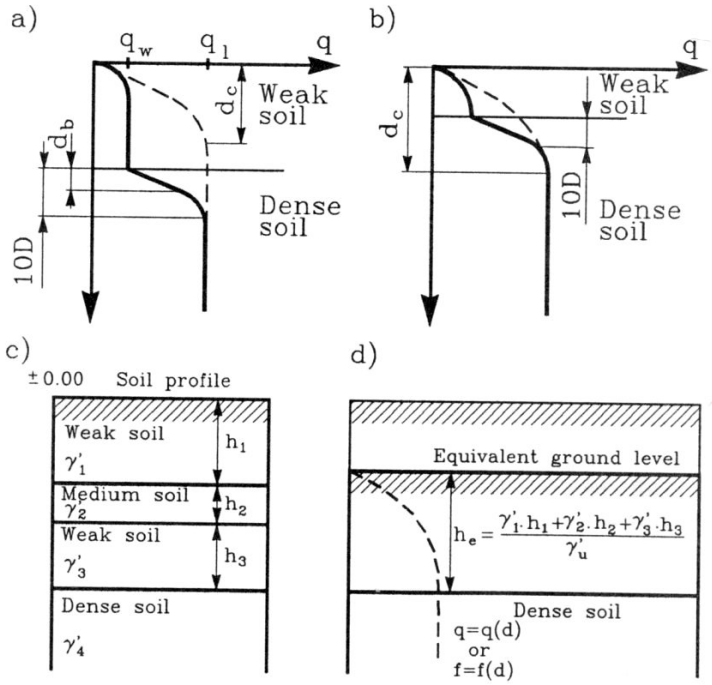

Figure 5.2: Ultimate bearing capacity of a pile. a) and b) Meyerhof's assumption. c) and d) equivalent ground level for base and shaft resistance.

be the real depth. (Fig. 5.2a). If the weak layer is thin then the critical depth corresponds to the dense sand (Fig.5.2b).

It must always be reconsidered, if it is better to neglect the weak layer, recalculate the equivalent ground level (see Fig. 5.2c and d) or even to calculate negative skin friction from the layer.

5.1 Point resistance

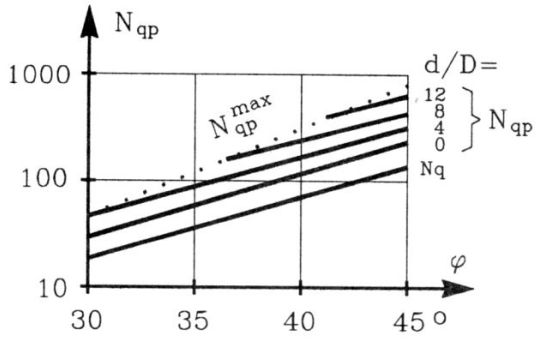

Figure 5.3: Bearing Capacity Factors for Driven Piles (Meyerhof, 1976).

The point resistance for sand q_p can be represented by

$$q_p = q'_v \, N_{qp} < q_l \tag{5.1}$$

where q'_v is the effective overburden pressure at pile tip. N_{qp} is a bearing capacity factor for point resistance. q_l is the limiting value corresponding to $d = d_c$. For driven piles N_{qp} is shown in Fig. 5.3 (bearing capacity factor for a strip footing) (square or circular cross section). N_q is shown too.

For piles penetrating shorter than 10D into the bearing stratum q_p may roughly be estimated by

$$q_p = q_N + \frac{(q_\ell - q_w) \cdot d_b}{10\,D} \approx \frac{q_\ell \cdot d_b}{10\,D} < q_\ell \tag{5.2}$$

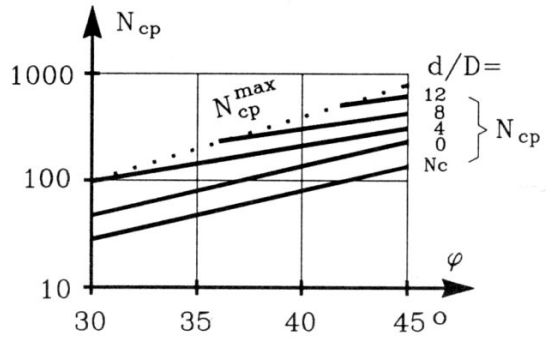

Figure 5.4: Bearing Capacity Factors for Driven Piles (Meyerhof, 1976).

corresponding to the situation in Fig. 5.2a.

If the bearing stratum covers a weak soil stratum, the thickness of the stratum below the pile tip should exceed 3-5 D in order to avoid penetration into the thin soil layer.

Point resistance in clay with cohesion c in the soil at pile tip level can be expressed by

$$q_p = c\, N_{cp} + q'_v\, N_{qp} \leq q_l \tag{5.3}$$

where q_l again corresponds to the critical depth. N_{cp} is shown in Fig. 5.4.

5.2 Shaft resistance in clay

The effective shaft resistance f' can be expressed as

$$f' = K \cdot \tan\delta \cdot \sigma'_{vo} = \beta \cdot \sigma'_{vo} < f_c \tag{5.4}$$

where K is an earth pressure coefficient, δ is the effective angle of friction between soil and pile shaft and σ'_{vo} is the average effective overburden pressure along the shaft (Burland (1973), Meyerhof (1977), NGI (1977)).

Close to the pile the soil is remoulded during installation and it therefore seems reasonable to use residual soil parameters and $\delta = \varphi'_{res}$.

It is, however, much more complicated to argue for a certain value of the K-parameter.

For bored piles the earth pressure at rest may be used. In normally consolidated clays

$$K \sim K_o = 1 - \sin\varphi' \approx 0.5 \tag{5.5}$$

whereas in preconsolidated clays

$$K_o = (1 - \sin\varphi')\sqrt{OCR} \leq 3 \tag{5.6}$$

OCR is the overconsolidation ratio. The maximum value of K_o corresponds to the passiv earth pressure coefficient. In the stiff, preconsolidated London Clay K_o ranges from about 3 at the ground level to 1 at great depth. For driven piles the volume displacement along the shaft causes K to increase, even up to the passive earth pressure coefficient. For a normally consolidated clay the average value of K varies from roughly K_o to more than 2 K_o. For a preconsolidated clay some part of the passive earth pressure is already developed and K varies therefore only up to 1.5 K_o.

Table 2. β-values for pile length < 15 m.

Bored piles, soft, normally consolidated clay	β	=	0.2 - 0.3
Driven piles, soft, normally consolidated clay	β	$\simeq$	0.3
Bored piles, stiff clay	β	=	0.5 - 1.5
Driven piles, stiff clay	β	$\simeq$	1 - 2.5

The length of the pile plays a role too. It may be explained by progressive mobilization of the skin friction due to compression of a long, elastic pile.

Fig. 5.5 shows the reduction of β for soft or medium clays.

F'_L in Fig. 5.5 should be used in the formula:

$$\beta_{reducted} = \beta \cdot F'_L \tag{5.7}$$

but only for soft or medium clays.

It is difficult to find a reasonable value for β in stiff clay.

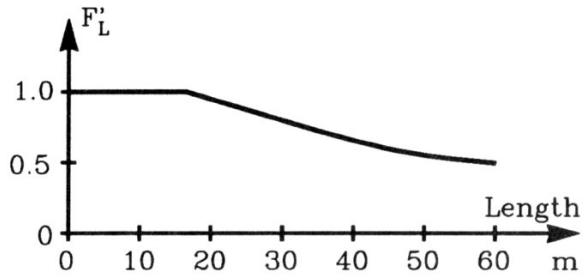

Figure 5.5: Reduction of β with length of pile (Driven piles in soft and medium clays).

5.3 Shaft resistance in sand

Formula (5.4) can be used again. Only some considerations on the value of K should be done.

In the Danish code it is proposed that

$$K \tan\delta = N_m = 0.6 \qquad \text{in compression}$$

but the exact value depends on such factors as procedures of pile installation, type of drilling, geometry of pile etc.

Chapter 6

Vertical settlements of a pile

The actual load on the pile develops shaft resistance and tip resistance. The shaft transfers some part of the load into the soil from near the ground surface to a great depth, where the soil also is carrying the load from the tip. It is difficult to calculate the settlement of a pile in one operation because the stress-settlement curve for the shaft differs a lot from that of the pile tip. Fig. 6.1 shows the development in total load Q, point resistance Q_p and shaft resistance Q_m as the settlement goes on. The shaft resistance is already fully developed when the settlement s exceeds s_c, but the point load is still increasing.

A settlement analysis for a pile therefore comprises two parts, a calculation of the shaft resistance and the point resistance corresponding to different values of s. The Q curve can then be drawn and the settlement corresponding to the actual load can be found.

6.1 Shaft resistance

The development of shaft resistance with settlement can be studied by laboratory tests with small models or analysed from back-calculation of pile tests.

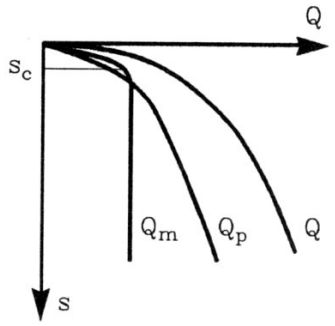

Figure 6.1: Load-settlement curve for a pile.

The result is given as so-called $f - z$ curves (Fig. 6.2) where f is Q_m/A_m and w_z is the vertical movement in mm.

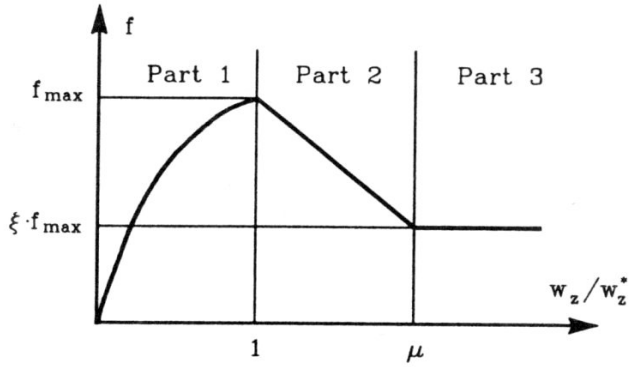

Figure 6.2: $f - z$ curve.

The curve shows a maximum point and a residual value described by the parameter ξ. The deformations take place in a very narrow zone along the surface and the strains get very big. Therefore, the clay along the surface will be remoulded and the shaft resistance drops down to its

residual value. The factor ξ depends on the soil and perhaps on the depth too.

Since the width of the zone is unknown, it is not possible to calculate strains in the soil. The movement can be dimensionless by dividing with the movement w_z^* corresponding to f_{max}. w_z^* depends on the soil and the roughness of the soil surface. See Table 6.1.

Table 6.1. Test results from AUC, K. Gwizdała.

Soil Type	Pile type	σ'_{vo} (kPa)	w_z^*/D (%)
clay	installed smooth	0 - 640	$1.33 + 0.14 \left(\frac{\sigma'_{vo}}{\sigma_a}\right)$
clay	installed rough	0 - 640	$2.92 + 0.25 \left(\frac{\sigma'_{vo}}{\sigma_a}\right)$
moraine clay	installed and driven, smooth	0 - 640	$0.46 - 0.001 \left(\frac{\sigma'_{vo}}{\sigma_a}\right)$
moraine clay	installed rough	0 - 640	$8.16 + 0.11 \left(\frac{\sigma'_{vo}}{\sigma_a}\right)$

Notes: $\sigma_a = 100kPa$
σ_{vo} kPa
pile diameter – 25.8 mm, smooth
pile diameter – 28.6 mm, smooth

The $f - z$ curve can be divided into three parts.

Part 1 shows a f increasing with the settlement. The initial tangent has been estimated by elastic solutions assuming pure shear in vertical planes. It should not be mentioned here, because it is a complicated theory which do not reflect the fact that the $f - z$ curve is totally dominated of movement along the surface in a very narrow zone.

A mathematical description of the curve in part 1 can be

$$f/f_{max} = (w_z/w_z^*)^{\beta^*} \tag{6.1}$$

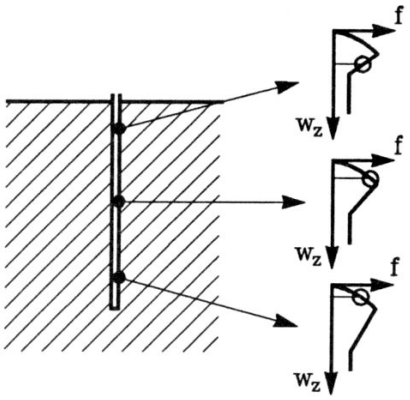

Figure 6.3: Reduction of f at long elastic piles.

where β^* is the only new parameter which have to be estimated from tests and shows to depend on the soil and the surface roughness of the pile.

In part 2 the shaft resistance drops down to its residual value, which is assumed to be constant when w_z exceeds μw_z^*. Part 2 is assumed to be a straight line for simplicity reasons. It sometimes shows to be curved.

So when describing an $f - z$ curve it could be done using four parameters ξ, μ, w_z^* and β^*.

f_{max} must be in accordance with the analysis of bearing capacity of the pile (part 4 and 5).

If the pile is very long the stiffness of the pile must be taken into consideration too. Near the pile tip the settlement along the surface and the settlement of the pile tip are nearly the same, but in smaller depths the elasticity of the pile increases the settlement. The settlement w_z^* corresponding to the maximum point could then be exceeded and f reduced.

In Table 6.1 - 6.4 some values estimated from laboratory tests carried out by students and K. Gwizdala at the AUC is given.

Table 6.2. Test results from AUC, K. Gwizdała.

Soil type	Pile type	σ'_{vo} (kPa)	β^* in formula (6.1)
clay	installed smooth	0 - 640	$\beta^* = 0.467 + 0.030 \left(\frac{\sigma'_{vo}}{\sigma_a}\right)$
	installed rough	0 - 640	$\beta^* = 0.514 + 0.00034 \left(\frac{\sigma'_{vo}}{\sigma_a}\right)$
moraine clay	installed and driven smooth	0 - 640	$\beta^* = 0.424 + 0.063 \left(\frac{\sigma'_{vo}}{\sigma_a}\right)$
	installed and driven rough	0 - 640	$\beta^* = 0.272 + 0.019 \left(\frac{\sigma'_{vo}}{\sigma_a}\right)$

Notes: $\sigma_a = 100!kPa$
σ'_{vo} (kPa)
pile diameter – 25.8 mm, smooth
pile diameter – 28.6 mm, rough

Table 6.3. Test results from AUC (K. Gwizdala).

Soil type	Pile type	σ'_{vo} [kPa]	ξ	μ
clay	installed smooth	0-640	$0.797 - 0.0024 \left(\frac{\sigma'_{vo}}{\sigma_a}\right)$	$11.15 - 0.57 \left(\frac{\sigma'_{vo}}{\sigma_a}\right)$
clay	installed rough	0-640	$0.654 - 00.39 \left(\frac{\sigma'_{vo}}{\sigma_a}\right)$	$6.41 - 0.40 \left(\frac{\sigma'_{vo}}{\sigma_a}\right)$
moraine clay	installed smooth	0-640	$0.802 - 0.03 \left(\frac{\sigma'_{vo}}{\sigma_a}\right)$	$22.30 - 0.22 \left(\frac{\sigma'_{vo}}{\sigma_a}\right)$
moraine clay	driven smooth	0-640	$0.599 - 0.015 \left(\frac{\sigma'_{vo}}{\sigma_a}\right)$	$12.97 - 0.13 \left(\frac{\sigma'_{vo}}{\sigma_a}\right)$
moraine clay	installed rough	0-640	$0.812 - 0.018 \left(\frac{\sigma'_{vo}}{\sigma_a}\right)$	$3.73 + 0.31 \left(\frac{\sigma'_{vo}}{\sigma_a}\right)$
moraine clay	driven rough	0-640	$0.585 - 0.015 \left(\frac{\sigma'_{vo}}{\sigma_a}\right)$	$11.92 + 0.65 \left(\frac{\sigma'_{vo}}{\sigma_a}\right)$

Notes: $\sigma_a = 100kPa$
pile diameter – 25.8 mm, smooth
pile diameter – 28.6 mm, rough

Table 6.4. Test results from AUC (pile diameter 50 mm)

test no.	σ'_v	s_u kPa	α	f_{max} kPa	w_z^* mm	ξ	μ
1	100			21.5	0.28	0.85	13.1
2	200	80	0.41	32.5	0.57	0.86	14.8
3	400	160	0.35	55.2	0.32	0.79	23.2

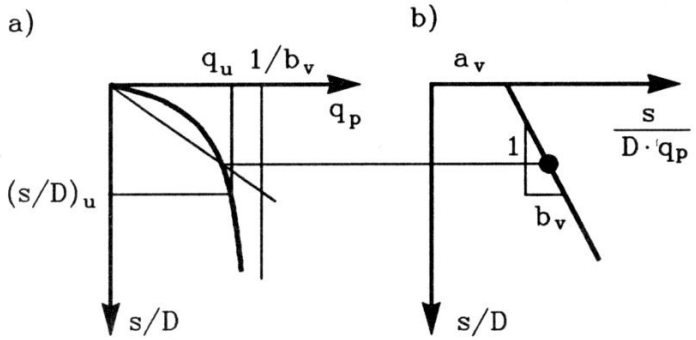

Figure 6.4: Load-settlement curve for pile tip.

6.2 Settlement of pile tip

A typical load-settlement curve for the pile tip is shown in Fig. 6.4 a. The base resistance q_p increases with increasing settlements, but more and more slowly. Q_p does not reach a maximum value and no residual state occurs. The reason is that when the piles move down, still new and undisturbed soilmasses are involved in the plastic zone and the strains are then rather small compared to the settlement of the pile.

The curvature must be described by a formula. A common used formula is

$$\frac{s/D}{q_p} = a_v + b_v \cdot s/D \tag{6.2}$$

called the hyperbolic type. The inclination of a sequant is then increasing linearly with the relative settlement.

For small values of s/D , the settlement modulus $1/a_v$ can be estimated from the theory of elasticity, from CPT-tests or pressiometer tests.

The parameter b_v can easily be estimated from pile loading tests, but pile loading tests are normally not by hand.

By writing formula (6.2) as:

$$q_p = \frac{s/D}{a_v + b_v \cdot s/D} \tag{6.3}$$

it is seen that $q_p \to 1/b_v$ for $s/D \to \infty$. Normally the ultimate load q_u is defined corresponding to a certain value of $s/D = (s/D)_u$.

A new and more convenient parameter v can be introduced by

$$\frac{1}{b} = v \cdot q_u \tag{6.4}$$

Fig. 6.4 shows that v depends on $(s/D)_u$. $1 \leq v \leq 1.5$ normally. By using (6.3) and (6.4):

$$q_u = \frac{1}{v \cdot b_v} = \frac{(s/D)_u}{a_v + b_v \cdot (s/D)_u}$$

$$\text{or} \quad (v-1) = \frac{a_v}{b_v (s/D)_u}$$

Formula (6.2) can then be expressed

$$\frac{s/D}{q_p} = a_v \left[1 + \frac{1}{v-1} \cdot \frac{s}{s_u}\right] \tag{6.5}$$

v should then be chosen to a value rather close to one, for instance 1.25 and s_u (which in this particular case is the ultimate settlement) could be chosen to 0.05 D for driven piles and 0.10 D for bored piles.

6.3 Calculation of settlement

The $t - z$ and $q - z$-curves (fig. 6.5) can be used for the determination of the load-settlement relationship for base $Q_p - s$, shaft $Q_s - s$ and total load $Q - s$, respectively.

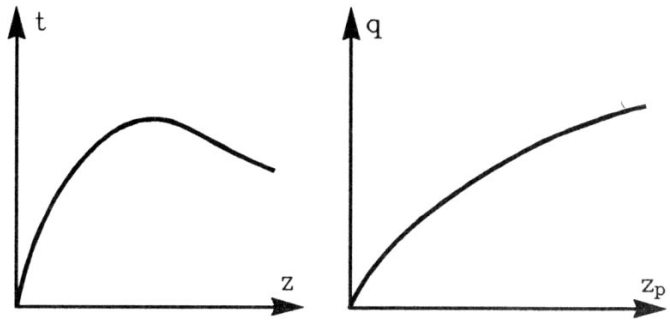

Figure 6.5: Load-settlement relationship for the single pile.

This problem was first presented in a paper by Coybe and Reese, 1966, proposing the following procedure:
- assume a small base movement, z_p
- compute Q_p according to z_p (see fig.6.6), then

$$\begin{aligned} Q_3 &= Q_p + S_{3p} \\ S_{3p} &= t_{3p} \cdot \pi \cdot D \cdot \Delta L \end{aligned}$$

where t_{3p} is determined from fig. 6.5, first with $z = z_p$ and then recalculated.

$$\begin{aligned} \Delta z_{3_p} &= \frac{0.5\,(Q_m + Q_p) \cdot 0.5 \cdot L_{3p}}{A \cdot E} \\ Q_m &\approx 0.5\,(Q_3 + Q_p) \\ z_{3p} &= \Delta z_{3p} + zp \\ &\vdots \end{aligned}$$

- go to the next segment above the bottom segment and work up the pile to compute a value of q_o and s at the top.

A more modern way of calculation is mentioned in chapter 8 – the finite difference method – but also finite element or similar methods may be used.

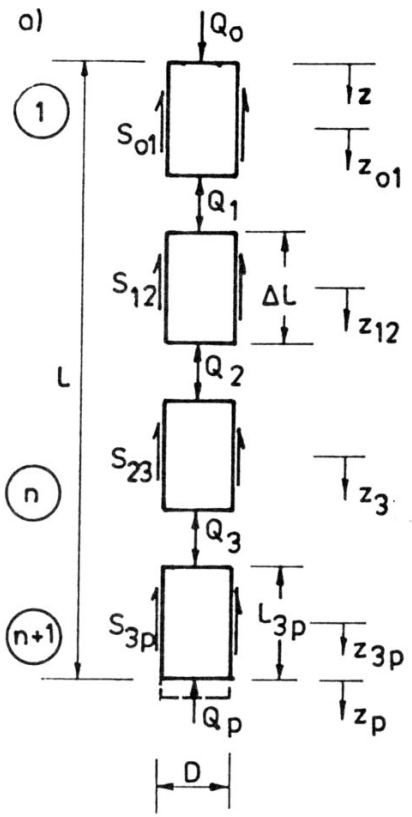

Figure 6.6: Model of pile for numerical calculation.

Chapter 7

Horizontal resistance of a pile

The analysis of the behaviour of laterally loaded piles is very important in construction of many offshore installations and foundations for big bridges crossing waters with waves, drifting ice floes and ricks for ship impact.

The analysis in offshore technique as recommended by the American Petroleum Institute (API) is based on some (a few) pile loading tests with large diameter piles and some theoretical considerations. Therefore, this chapter will include the API recommendations and compare them with more consistent theories.

The ultimate horizontal resistance of a pile can be determined from the theory of plasticity although it is not possible to find a kinematically admissible solution for a pile in sand.

If a pile is moved horizontally the upper part of the pile will press the body of soil up to the surface whereas in greater depths the soil will move around the pile in horizontal planes. It is assumed that only these two failure modes occur:

1. *In moderate depths* the soil will move to the surface.
2. *In great depths* the soil will move around the pile.

If the pile rotates about a point at a certain depth d_R below the ground surface it is assumed that the two failure modes also apply in this case.

Since the soil close to the pile surface always is disturbed to some extent the pile will – on the safe side – be considered as smooth.

7.1 Horizontal resistance in clay, great depth

In great depths the soil flows around the piles in horizontal planes during failure. The undrained failure takes place at constant volume which makes it possible to make statically and kinematically admissible solutions.

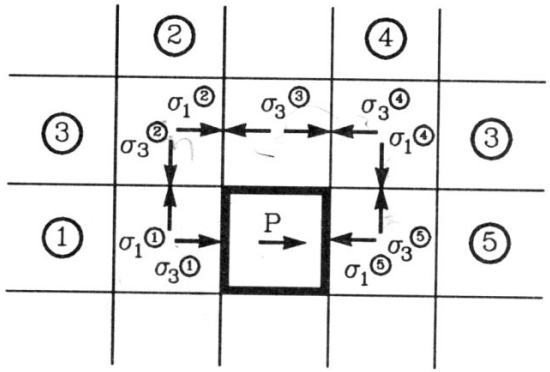

Figure 7.1: A lower bound solution of horizontal resistance in clay. Great depth.

A simple static solution can be obtained from Fig. 7.1 using stress bands (with numbers in superscript). At the back of the pile the normal stress is assumed to be zero:

$$\sigma_3^1 = 0$$

$$\sigma_1^1 = 2s_u = \sigma_3^2$$

$$\sigma_1^2 = 4s_u = \sigma_3^3 = \sigma_3^4$$

$$\sigma_1^4 = 6s_u = \sigma_3^5$$

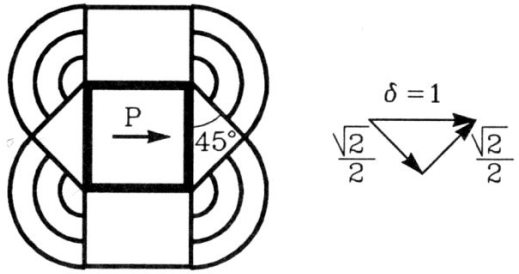

Figure 7.2: An upper bound solution of horizontal resistance in clay. Great depth.

$$p = \sigma_1^5 = 8s_u = N_c^p s_u$$

This is a lower limit for p. Using inclined stress band a higher value of N_c^p can be determined showing that

$$N_c^p > 10 \tag{7.1}$$

A simple upper bound solution which might be correct is shown in Fig. 7.2. The pile and two triangular bodies covering the front and the back of the pile moves $\delta = 1$. Two components of δ are important. $\sqrt{2}/2$ is taken as shear movements along the surface of the triangles and $\sqrt{2}/2$ causes parallel movement in the four radial zones and a stiff body movement along the sides of the piles.

The result is

for a rough square pile	$p = 16.25\ s_u$	
for a smooth square pile	$p = 12.83\ s_u$	(7.2)

A similar solution can be obtained for a cylindrical pile when the cross section of the pile is changed to a square with the same area:

for a smooth, cylindrical pile	$p = 10\ s_u$	(7.3)

API recommends for a cylindrical pile

$$p = 9\ s_u \tag{7.4}$$

which is nearly correct.

7.2 Horizontal resistance in clay, moderate depth

When a smooth pile moves horizontally the passive earth pressure E_p on the front of the pile can be determined correctly (Fig. 7.3):

$$E_p = 2s_u Bd + \sqrt{2}d^2 s_u + \frac{1}{2}\gamma_m B d^2$$

and

$$p_p = \frac{1}{B}\frac{\partial E}{\partial d} = 2s_u + 2\sqrt{2}\frac{d}{B}s_u + \gamma_m d \qquad (7.5)$$

either by projecting all forces on the failure plane or by using the equation of virtual work.

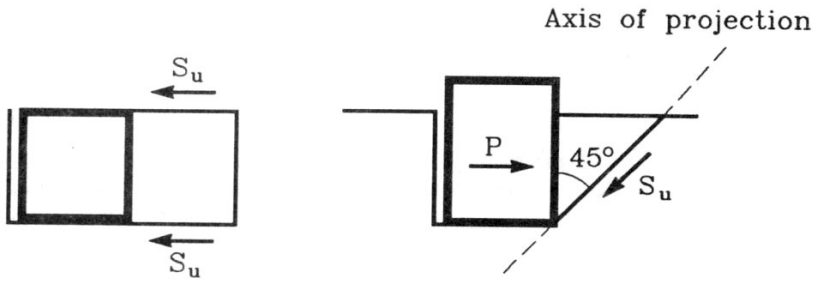

Figure 7.3: State of equilibrium for a smooth pile.

The corresponding active pressure p_a on the back of the pile is :

$$p_a = -2s_u - 2\sqrt{2}\frac{d}{B}s_u + \gamma_m d \qquad (7.6)$$

Fissure along the back side of the pile.[

If $p_a < 0$ the active pressure will not develop and a fissure appears. If $p_a = 0$ at a certain depth the fissure will close and disappear at that depth. If p_a remains negative with increasing depth the fissure will close at the transition depth d_t where the new failure mode develops.

d_t can be determined from formula (7.2) and (7.5):

$$12.8s_u = 2s_u + 2\sqrt{2}\frac{d}{B}s_u + \gamma_m d$$

$$\frac{d_t}{B} = \frac{10.8}{\frac{\gamma_m B}{s_u} + 2\sqrt{2}} \qquad (7.7)$$

The relative depths of fissure d_s/B and transition d_t/B depend only on the dimensionless parameter $\gamma_m B/s_u$, see Fig. 7.4.

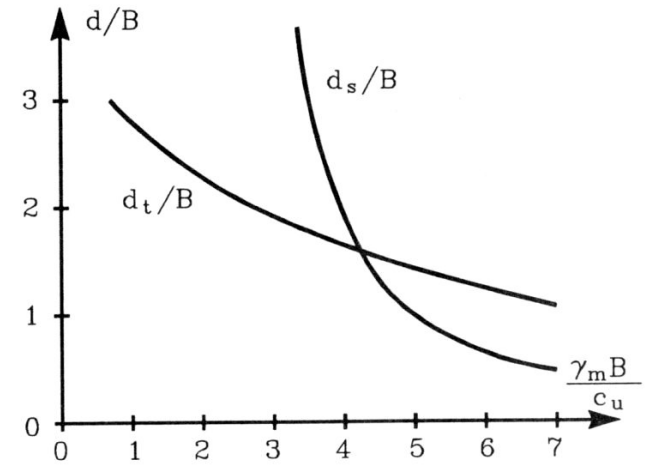

Figure 7.4: Relative depth of fissure d_s/B and relative depth of transition d_t/B versus $\gamma_m B/s_u$.

When $\gamma_m B/s_u = 4.11$, then $d_s = d_t$.
When $d < d_s < d_t$ the resistance p is determined by formula (7.5).
Fig. 7.5 shows two examples of failure modes.
When $d_s < d < d_t$ (or $\gamma_m B/s_u > 4.11$) the resistance p is determined

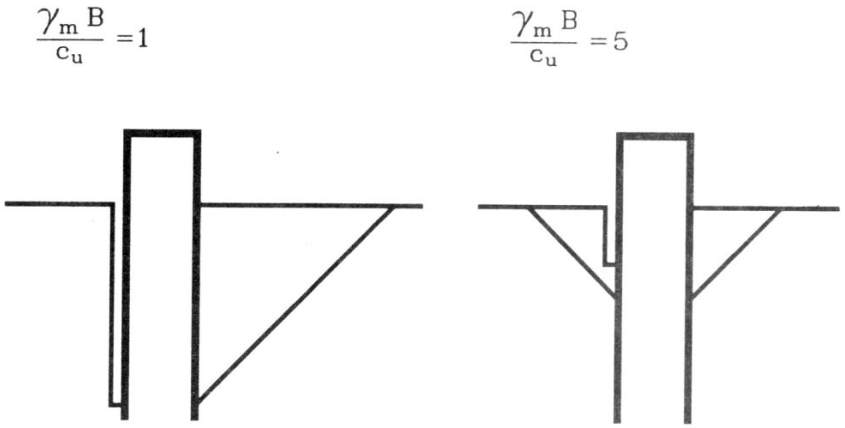

Figure 7.5: Examples of failure modes in moderate depth.

by:

$$p = p_p - p_a = 4s_u + 4\sqrt{2}\frac{d}{B}s_u \tag{7.8}$$

When $d_t < d$ then formula (7.2) can be used: $p = 12.8\ s_u$.

Matlocks solution.

Mathlock (1970) uses the following equation which appears to describe the variation of the horizontal resistance with a satisfactory degree of approximation

$$p = N_p \cdot s_u$$

where

$$N_p = 3 + \frac{\gamma_m d}{s_u} + 0.5 \cdot \frac{d}{B} \tag{7.9}$$

It is not possible to argue in favour of this formula from a theoretical point of view.

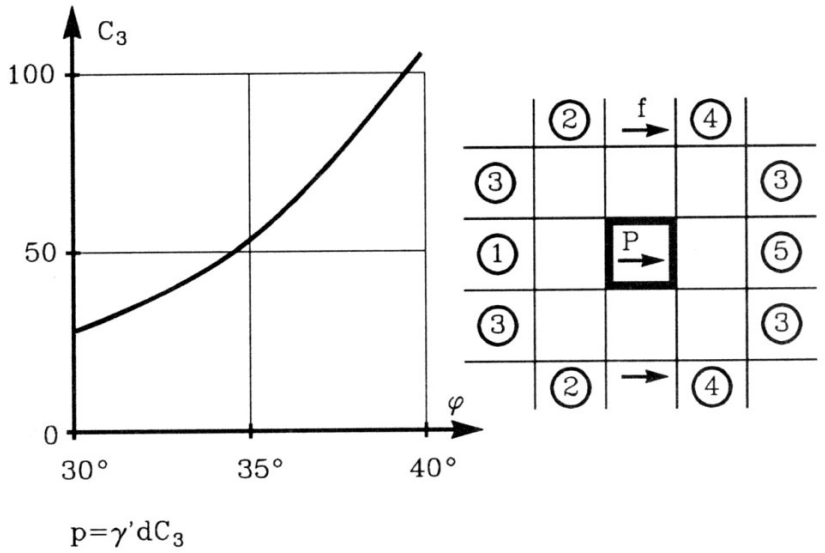

Figure 7.6: Horizontal resistance of a pile element in great depth. Reeses solution.

7.3 Resistance in sand, great depth

It is not possible to present an upper bound solution for the horizontal resistance of a pile element in frictional material since volume increments take place and force the plastic body to expand into the surrounding elastic body (Fig. 1.3b).

However, a lower bound solution is easily obtained (Fig. 7.6). At the back of the pile the stress state corresponds to the active earth pressure pK_a. Following the normal principal stresses around the pile the stresses increase as follows (with the stress band numbers in superscript):

$$\sigma_3^1 = \gamma' dK_a$$

$$\sigma_1^1 = \gamma' dK_a \, tan^2(45 + \frac{\phi}{2}) = \sigma_3^2$$

$$\sigma_1^2 = \gamma' dK_a \, tan^4(45 + \frac{\phi}{2}) = \sigma_3^3$$

$$\sigma_1^3 = \gamma' dK_a \, tan^6(45 + \frac{\phi}{2}) = \sigma_3^4$$

$$\sigma_1^5 = \gamma' dK_a \, tan^8(45 + \frac{\phi}{2})$$

$$p = \sigma_1^5 - \sigma_3^1 = \gamma' dK_a \cdot (tan^8(45 + \frac{\phi}{2}) - 1) \qquad (7.10)$$

Reese proposed to take a frictional force f into account on the surface of band No. 3 (Fig. 7.6) which moves relatively to the surrounding soil. The normal stress on the border of band No. 3 corresponds to the earth pressure at rest $\gamma' dK_o$ and $f = \gamma' dK_o \, tan\phi$. Reese found:

$$p = \gamma' dK_a(tan^8(45 + \frac{\phi}{2}) - 1) + \gamma' dK_o tan\phi \, tan^4(45 + \frac{\phi}{2}) \qquad (7.11)$$

or remembering that $K_a = tan^2(45 - \phi/2)$ and $K_o \simeq 0.5$:

$$p = \gamma' d[(tan^6(45 + \frac{\phi}{2}) - tan^2(45 - \frac{\phi}{2})) + 0.5 \, tan\phi \, tan^4(45 + \frac{\phi}{2})] \qquad (7.12)$$

Brinch Hansen (1961) has proposed:

$$p = \bar{q} K_q^\infty = \bar{q} \cdot N_c d_c^\infty K_o \, tan\phi$$

or

$$p = \gamma d K_o (1.58 - 4.09 \, tan^4\phi_{pl}) \, (e^{\pi tan\phi_{pl}} \, tan^2(45 + \frac{\phi_{pl}}{2}) - 1) \qquad (7.13)$$

where ϕ_{pl} corresponds to the plane state and can be determined as $\phi_{pl} = 1.1 \, \phi_{tr}$. K_o is proposed to be $(1 - sin\phi)$. Brinch Hansens equation has been demonstrated by model tests.

ϕ	Reese	ϕ_{pl}	Brinch Hansen
30	29.3	33	26.4
35	54.7	38.5	62.3
40	105.9	44	179

Table 7.1: $p/\gamma d$: Comparison of formulas (7.11) and (7.13).

Formula (7.11) is adapted by API and it is apparently on the safe side.

The resistance P per m pile in a depth d can be expressed as:

$$P = \gamma' dB \quad \text{for a square pile or}$$

$$P = \gamma' dD \quad \text{for a cylindrical pile} \qquad (7.14)$$

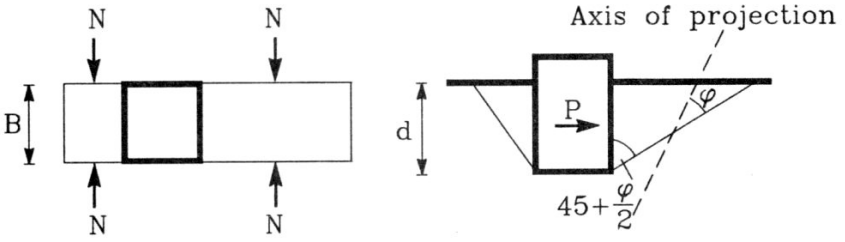

Figure 7.7: Brinch Hansens solution for a smooth pile. Moderate depth.

7.4 Resistance in sand, moderate depth

Ultimate resistance. Lower bound solution.

Brinch Hansen (1961) considered the static equilibrium of a wedge which moves forward and upward when the pile deflects horizontally (Fig. 7.7).

The shape of the wedge corresponds to the simplest possible case, the passive Rankine failure state which might occur when the pile surface is smooth.

The weight of the wedge is:

$$W = \frac{1}{2}\gamma d^2 B \, tan(45 + \frac{\phi}{2}) \tag{7.15}$$

Forces N are acting on the vertical sides of the wedge corresponding to earth pressure at rest

$$N = \frac{1}{6}\gamma d^3 K_o \, tan(45 + \frac{\phi}{2}) \tag{7.16}$$

During failure a frictional force $N \, tan\phi$ acts on the vertical surfaces of the wedge.

Projecting all forces acting on the wedge into a plan perpendicular to the total force at the under side of the wedge the total horizontal force P_p is obtained

$$P_p = \frac{1}{2}\gamma' d^2 B tan^2(45 + \frac{\phi}{2})[1 + \frac{2}{3}\frac{d}{B} K_o \frac{sin\phi}{sin(45 + \frac{\phi}{2})}]$$

The passive unit horizontal resistance $P_p(kPa)$ is then

$$P_p = \frac{1}{B}\frac{\partial P_p}{\partial d} = \gamma' d \, tan^2(45 + \frac{\phi}{2})[1 + \frac{d}{B} K_o \frac{sin\phi}{sin(45 + \frac{\phi}{2})}] \tag{7.17}$$

Brinch Hansen neglected the active horizontal resistance P_a but it is very easily taken into account by changing the sign of ϕ:

$$P_a = \gamma d \, tan^2(45 - \frac{\phi}{2})[1 - \frac{d}{B} K_o \frac{sin\phi}{sin(45 + \frac{\phi}{2})}] \tag{7.18}$$

and then

$$P = P_p - P_a \tag{7.19}$$

This formula will be used in the following text.

Ultimate resistance, upper bound solution.

A kinematically admissible solution requires another shape of the wedge.

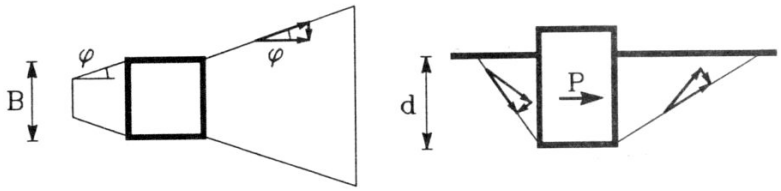

Figure 7.8: Movements in a kinematically admissible solution for a smooth pile. Moderate depth.

Assuming the normality rule to hold, the frictional shearing is followed by volume increments (dilatancy) (Fig. 7.8).

The movement of the wedge does not follow the under side of the wedge but follows a more vertical direction (Fig. 7.8).

Moving the pile $\delta = 1$ in the horizontal direction and remembering that the shear force is perpendicular to the shear movements the equation of virtual work gives:

$$P = -\frac{1}{2}\gamma d^2(B + dcot(45 - \frac{\phi}{2})tan\phi)tan^2(45 + \frac{\phi}{2}) - (B - dcot(45 + \frac{\phi}{2})tan\phi)tan^2(45 - \frac{\phi}{2})$$

or

$$P = \frac{1}{B}\frac{\partial P}{\partial d} = tan^2(45 + \frac{\phi}{2}) - tan^2(45 - \frac{\phi}{2}) + \frac{3}{2}\frac{d}{B}[tan^3(45 + \frac{\phi}{2}) + tan^3(45 - \frac{\phi}{2})]tan\phi \tag{7.20}$$

including passive and active earth pressure.

Reeses solution.

Reese (1974) proposed the following formula which is based on static equilibrium of a wedge (Fig. 7.9).

$$P = \gamma d[\frac{K_o d tan\phi sin\beta}{tan(\beta - \phi)cos\alpha} + \frac{tan\beta}{tan(\beta - \phi)}(D + dtan\beta tan\alpha)$$

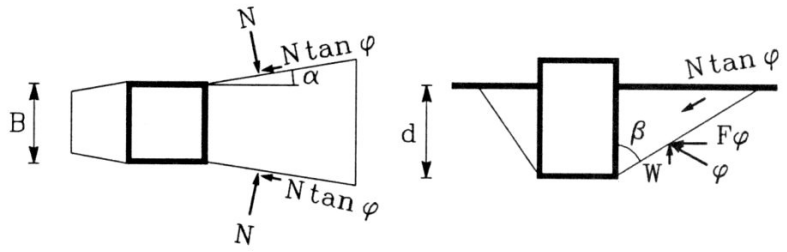

Figure 7.9: Reeses equilibrium solution for a smooth pile. Moderate depth.

$$+K_o d tan\beta(tan\phi sin\beta - tan\alpha) - K_a B] \tag{7.21}$$

which can be simplified by assuming $\beta = (45+\phi/2)$. If $\alpha = 0$ then formula (7.17) is valid but normally α is assumed to take values close to 0.5 ϕ. K_o is assumed to be 0.4 - 0.5.

Conclusion

The ultimate horizontal resistance p of a pile in sand at moderate depths can be expressed as:

$$p = \gamma d(C_1 \frac{d}{B} + C_2) \tag{7.22}$$

where B is the width of a square pile or the diameter of a cylindrical pile.

C_2 is the coefficient of earth pressure on a vertical, smooth wall subjected to active and passive pressure.

$$C_2 = tan^2(45 + \frac{\phi}{2}) - tan^2(45 - \frac{\phi}{2}) \tag{7.23}$$

which is the correct value of C_2.

C_1 is a coefficient which takes the limited length of the "wall" into consideration. Fig. 7.10 shows the upper bound solution and Brinch Hansens solution which is close to a lower bound solution.

API uses the coefficient argued by Reese and it takes appropriate values in the middle of the range. Thus, the API value of C_1 is recommended.

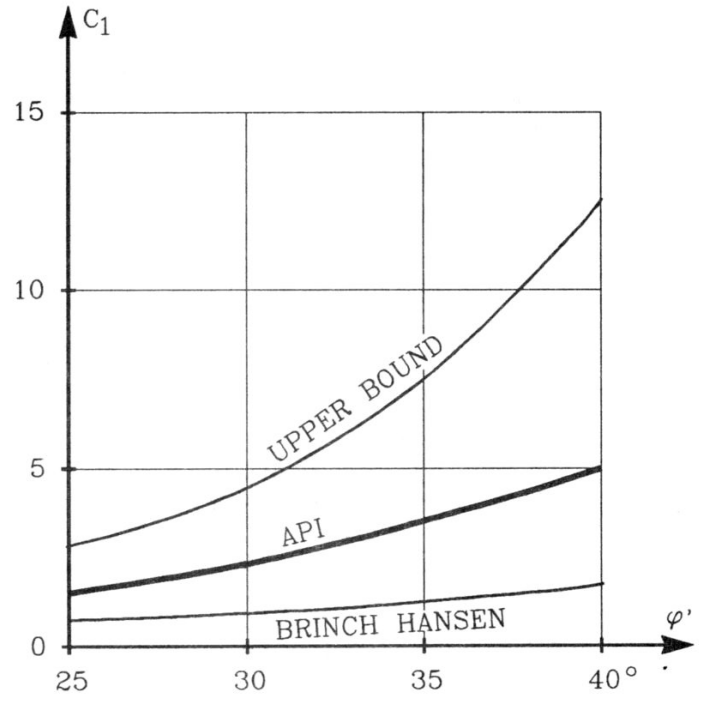

$$p = \gamma' d(C_1 \frac{d}{B} + C_2)$$

$$C_2 = \tan^2(45+\frac{\varphi'}{2}) - \frac{1}{\tan^2(45+\frac{\varphi'}{2})}$$

Figure 7.10: Coefficient C_1 as function of ϕ'.

7.5 Horizontal resistance of a pile

Fig. 7.11 shows a pile which is driven to a depth of d_m below the surface. The soil conditions are known. The ultimate value of the force H acting on the pile at a height a above the soil surface should now be determined.

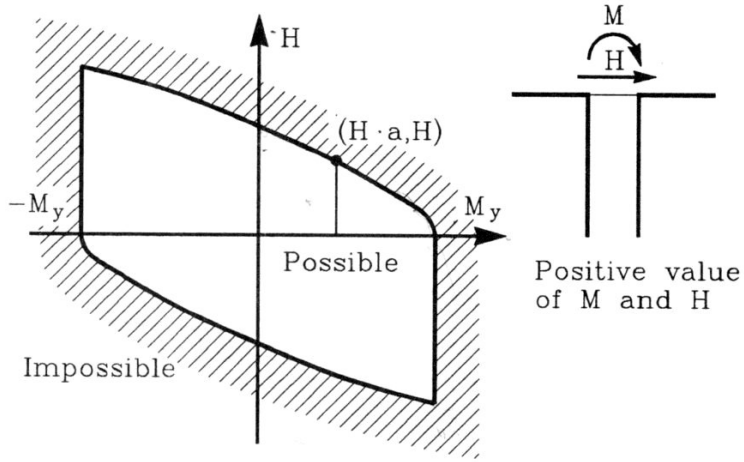

Figure 7.11: Possible combinations of H, M for a given pile.

The pile resistance, corresponding to a parallel and horizontal movement of the pile, is calculated by the earlier mentioned methods. In layered soil with sand and clay layers the actual values of s_u, γ_m and ϕ', γ' should be used. In the formulas concerning sand the term $\gamma' d$ should be replaced by the effective overburden pressure. The pile will rotate around a point at depth d_r and the resistance will change to the other side of the pile. d_r is fixed by trial in such a way that the two pressure areas give equal momentums above the line of the force H. The force H can be determined

by horizontal equilibrium. The maximum moment M_m exists in a depth d_o where the transversal force in the pile is zero. The cross section of the pile must be able to resist M_m.

The analysis of a given pile is easily extended to include a combination of H and M at the soil surface level. This is often useful in offshore technique. Fig. 7.11 shows an analysis with a pile which yields at a momentum of M_y. The possible combinations of H, M are inside the area with curved borders. The point (Ha, H) represents the calculation made in Fig. 7.12.

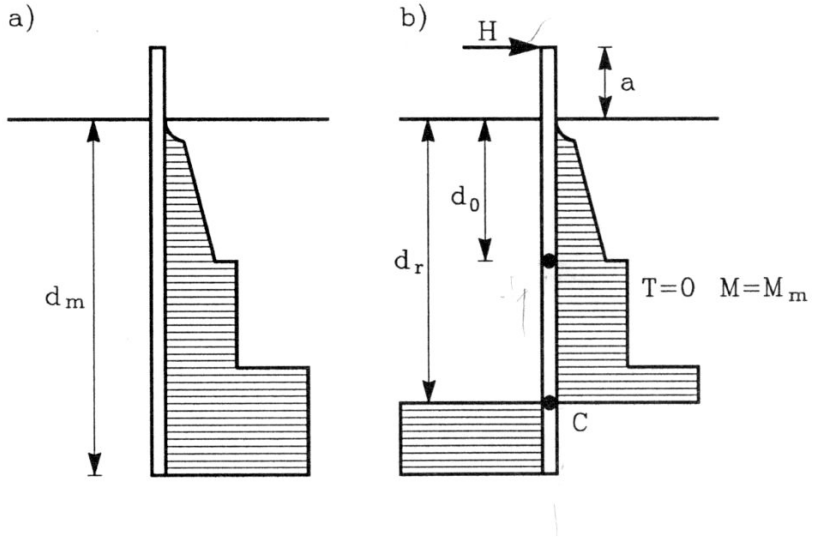

Figure 12: a) Earth pressure diagram. b) Horizontal resistance by rotating around C.

Chapter 8

Horizontal movements of piles

When a pile is loaded by a horizontal force in a hight a above the soil surface the pile top rotates and deflects laterally (Fig. 8.1). This respons of the pile may be of essential importance for the behaviour of the construction, which is subjected to horizontal forces.

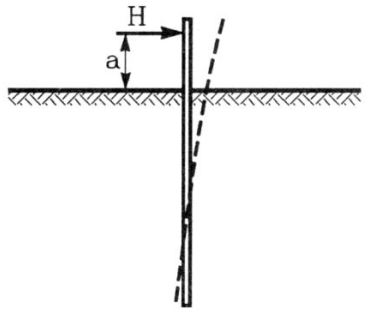

Figure 8.1: Horizontal force acting on a pile

The horizontal deflection w_y of a pile at a depth z is expressed by the well-known differential equation:

$$EI \frac{\partial^4 w_y}{\partial z^4} + N \frac{\partial^2 w_y}{\partial z^2} + E_s w_y = 0 \tag{8.1}$$

which tells that the sum of reactions on the pile causing the deflection of the pile itself, the axial load N and the movements of the pile into the soil is zero.

The pile is assumed to be elastic with a flexural stiffness of EI. The behaviour of the soil is expressed by the deflection modulus E_s (kPa).

The equation 8.1 with appropriate boundary conditions is easily solved by numerical methods, as for instance the finite difference method, mentioned in section 8.4.

The real problem is to determine the quantity E_s. If the soil is elastic with a constant modulus of elasticity E, it is possible, but complicated, to use a closed-form solution based on the Mindlin formula for a horizontal force Q acting beneath the surface of a semi-infinite elastic half-space (Fig. 8.2), i.e. an elastic solution of the pile-soil interaction.

However, such factors as variation of the soil modulus with depth or shear force or geometrical irregularities complicate the calculation and make close-formed solution impossible.

In order to facilitate the analysis the Winkler model is very useful. The soil is considered to consist of a series of independent soil layers with smooth horizontal boundaries. The soil resistance of such a layer can then be represented by a soil spring or even by a spring/dashpot system. The value of E_s could then be argued from the theory of elasticity.

McClelland et al. (1969) and Matlock (1970) proposed to use a so-called $p-y$ curve for each of this layers, which gives the soil resistance p as a function of the pile deflection w_y in the y-direction. The $p-y$ curves can be non-linear, they can have a maximum of p, and deflections in accordance with laboratory tests. A great deal of work has been done to develope the correct shape of $p-y$ curves. It is difficult because the only possibility of calibrating the curves is to compare calculations of the deflection and rotation of the pile top with measured values, and in the calculation of a single pile many $p-y$ curves have to be used.

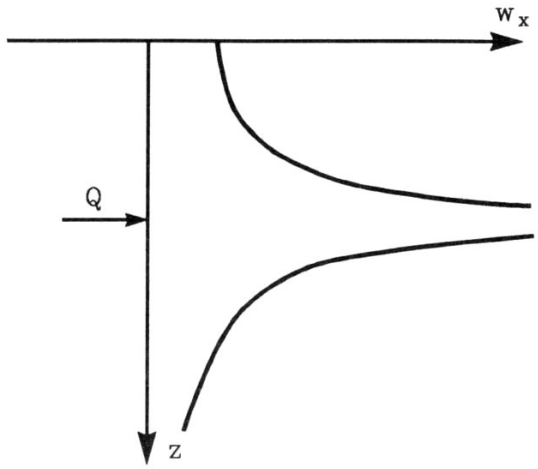

Fig. 8.2: Horizontal deflection w_x caused by a horizontal force Q acting beneath the surface of an elastic material (Mindlin solution).

8.1 Load deflection curves for soft clay

The shape of the load deflection or $p-y$ curve has been studied by means of extensive field testing with an instrumented pile, experiments with laboratory models and parallel development of analytical methods and correlations (Matlock 1970).

Three conditions of lateral load are of interest in offshore design: Short-time static loading, cyclic loading and subsequent reloading after cycling.

A $p-y$ curve is normally in non-dimensional form using y/y_c versus p/p_u. p_u is the ultimate resistance against horizontal movements and can be determined from methods mentioned in chapter 7. y_c is a characteristic deflection which according to Skempton is:

$$y_c = 2.5\,\varepsilon_c \cdot D \tag{8.2}$$

D is the pile diameter. ε_c is the strain which occurs at one-half the maximum stress in undrained compression tests on undisturbed soil samples. ε_s is normally assumed to be 0.005 for a stiff or brittle clay, 0.020 for very soft clays.

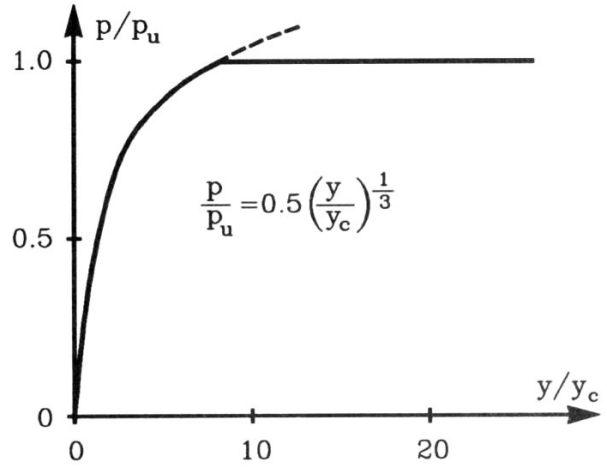

Figure 8.3: $p-y$ curve for short time static loading.

A $p-y$ curve for short-time static loading in soft clay is proposed to be expressed by

$$\begin{aligned} p/p_u &= 0.5\,(y/y_c)^{1/3} \qquad \text{for } y < 8y_c \\ p/p_u &= 1 \qquad\qquad\qquad\quad \text{for } y > 8y_c \end{aligned} \tag{8.3}$$

See also Fig. 8.3.

During cyclic loading the $p-y$ curve changes due to reduction in soil strength and remoulding of clay. In a final, stable state the failure load is assumed reduced to $0.72\,p_u$. The $p-y$ curve can then be expressed by

$$\begin{aligned} p/p_u &= 0.5\left(\frac{y}{y_c}\right)^{1/3} \qquad \text{for } y < 3y_c \\ p/p_u &= 0.72\left(\frac{d}{d_t}\right) < 0.72 \qquad \text{for } y > 15y_c \end{aligned} \tag{8.4}$$

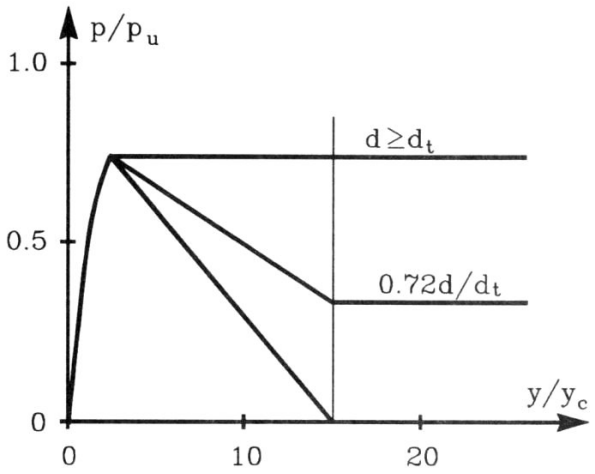

Figure 8.4: $p-y$ curve for cyclic loading in final, stable state.

and a linear variation between $y = 3y_c$ and $15y_c$. (Fig. 8.4) d_t is the transition depth where the failure mode changes from upwards plastic flow to a horizontal plastic flow around the pile.

An effect of cyclic loading appears to be a permanent displacement of the soil away from the pile creating fissures down along the pile and reducing the horizontal resistance. In formula $p/p_u \to 0$ for $d \to 0$.

When $d > d_t$ the plastic flow around the pile closes the fissures and the only effect of cyclic loading is then the reduction in strength.

The shape of the $p-y$ curve during cyclic loading depends on the depth d_t, where the failure mode changes from a wedge moving up to the soil surface to a plastic flow around the pile.

The fissures created by cyclic loading seem to be permanent. A $p-y$ curve in reloading after cyclic loading is therefore assumed to follow the rule given in Fig. 8.5.

These $p-y$ curves are recommended by API. It is the first serious attempt to describe the behaviour of a laterally moved pile segment.

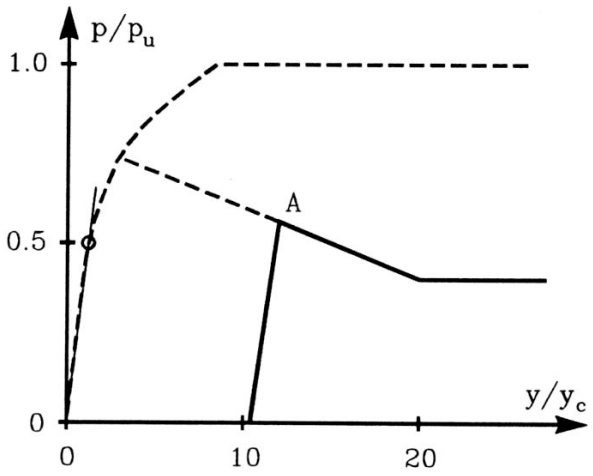

Figure 8.5: $p-y$ reloading curve after cyclic loading. Point A is the previous stable state of cyclic loading.

It is easy to improve the shape of the curves. The curves have vertical tangent for $y = 0$, and that corresponds to a total stiff soil at small loadings. Poulus (1982) has proposed to use, for small value of p, an inclining line with movements corresponding to an elastic soil. From the load where this line intersects the Matlock curve (Fig. 8.3), the curve should be used. It is also difficult to believe that the $p-y$ curve is unchanged during cyclic loading when $p/p_u < 0.72$.

The real advantage of using $p-y$ curves is the ability to describe the strongly inelastic behaviour of soils in a simple way, which also makes an analysis of the behaviour of a pile rather easy.

8.2 Load deflection curves for stiff clay

API do not recommend a particular shape of a $p-y$ curve for a stiff clay.

But stiff clays are generally more brittle than soft clays. In developing stress strain curves in triaxial testing and subsequent $p-y$ curves for cyclic loads, good judgements should reflect the rapid deterioration of load capacity at large deflections.

8.3 Load deflection curves for sand

The construction of $p-y$ curves for sand is based on the calculation of the ultimatic horizontal resistance of a pile corresponding to moderate depths p_{cm} and to great depths p_{cd} and the transition depth d_t where the failure mode changes from an upward plastic flow to a horizontal plastic flow around the pile.

The ultimate resistance p_c has been adjusted by comparing with observed soil resistance p_u and an empirical adjustment factor A has been introduced:

$$p_u = A \cdot p_c \tag{8.5}$$

where $A = 0.9$ for cyclic loading and $A = \left(3 - 0.8\frac{d}{D}\right) \geq 0.9$ for static loading.

The initial horizontal subgrade reaction E_j is for a friction material expressed by

$$E_j = k \cdot d \tag{8.6}$$

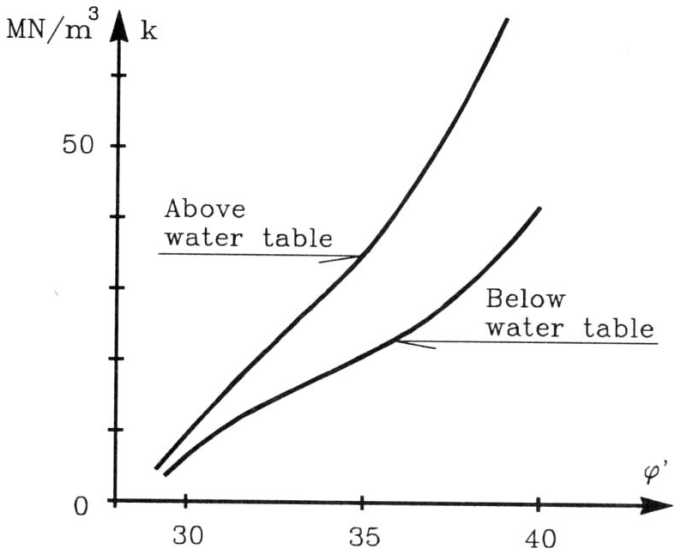

Figure 8.6: Initial modulus of subgrade reaction versus angle of internal friction φ'. Sand.

where k is a coefficient MN/m^3. k can be determined from Fig. 8.6, as recommended by API.

The $p-y$ curve may be approximated by

$$\frac{p}{p_u} = tanh\left(\frac{k \cdot d}{p_u} \cdot y\right) \tag{8.7}$$

in the absence of more definitive information (API).

A typical family of $p-y$ curves is shown in Fig. 8.7.

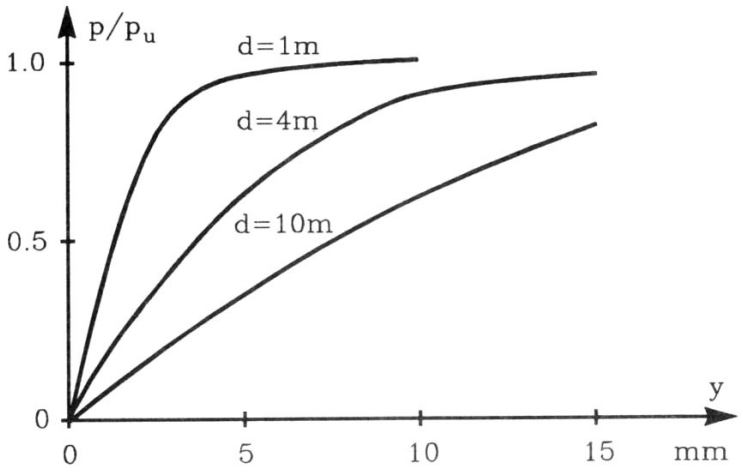

Figure 8.7: $p/p_u - y$ curves for sand: $\varphi' = 35°$. $\gamma' = 10\ kN/m^3$. $D = 0.5\ m$. Below water level.

Alternatively, the laboratory model tests results can be used for the determination of the type $p-y$ curve, for example hyperbolic curve, see fig. 8.8.

8.4 Movements of pile top at horizontal loads

The deflection of an elastic pile and the horizontal movement and distorsion of the pile top can now be calculated. In the differential equation (formula 8.1)

$$EI\frac{\partial^4 w_y}{\partial z^4} + N\frac{\partial^2 w_y}{\partial z^2} + E_s w_y = 0 \tag{8.8}$$

the quantity E_s, which describes the behaviour of the soil, is determined from the $p-y$ curves.

It is only possible to use elastic closed form solution if the variation of E_s is very simple as for instance if E_s varies linearly with depth.

The finite element method can in principle be used. A description of a three-dimensional solid element for soil and pile and an interface

element has been given, and a procedure for non-linear three-dimensional analysis has been described. The use of finite elements still seems to involve considerable human efforts and computer capacity.

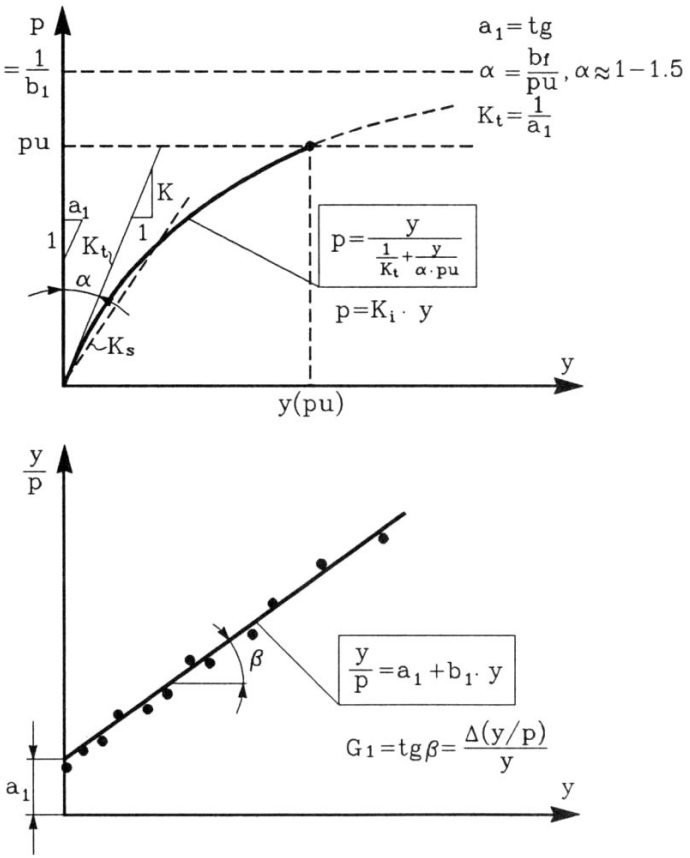

Figure 8.8: Horizontal movement of laterally loaded piles on the base laboratory tests.

The finite different method is still in use and is directly understandable. The pile is discretizised in a number of nodes (Fig.8.9), from bottom to top. Normally the distance h between the nodes is constant.

The horizontal deflections $w_{y,n}$ of the n nodes are unknown. The finite difference analog to various differential derivaties is given by

$$\left(\frac{\partial w_y}{\partial z}\right)_m = \frac{w_{y,m+\frac{1}{2}} - w_{y,m-\frac{1}{2}}}{h} \quad \text{or} \quad \frac{w_{y,m+1} - w_{y,m-1}}{2h} \tag{8.9}$$

$$\left(\frac{\partial^2 w_y}{\partial z^2}\right)_m = \frac{1}{h}\left(\left(\frac{\partial w_y}{\partial z}\right)_{m+\frac{1}{2}} - \left(\frac{\partial w_y}{\partial z}\right)_{m-\frac{1}{2}}\right)$$

$$= \frac{1}{h^2}\left(w_{y,m+1} - 2w_{y,m} + w_{y,m-1}\right) \tag{8.10}$$

In the same way is obtained

$$\left(\frac{\partial^3 w_y}{\partial z^3}\right)_m = \frac{1}{2h^3}\left(w_{y,m+2} - 2w_{y,m+1} + 2w_{y,m-1} - w_{y,m-2}\right) \tag{8.11}$$

$$\left(\frac{\partial^4 w_y}{\partial z^4}\right)_m = \frac{1}{h^4}\left(w_{y,m+2} - 4w_{y,m+1} + 6w_{y,m} - 4w_{y,m-1} + w_{y,m-2}\right) \tag{8.12}$$

Formula (8.8) combined with (8.10) and (8.12) gives n equations. It is possible to change the values of EI and N for each point but they are normally assumed to be constant.

A closer view on the system of equations shows that there are $n+4$ unknown quantities. The last four unknowns are $w_{y,n+1}$ $w_{y,n+2}$ $w_{y,0}$ and $w_{y,-1}$ corresponding to non-existing point (phantom points). The boundary conditions in terms of $\partial y/\partial x$ (slope of pile), $\partial^2 y/\partial x^2$ (moment) and $\partial^3 y/\partial x^3$ (shear) are expressed by using the phantom points. EI of the phantom points is assumed to be unchanged.

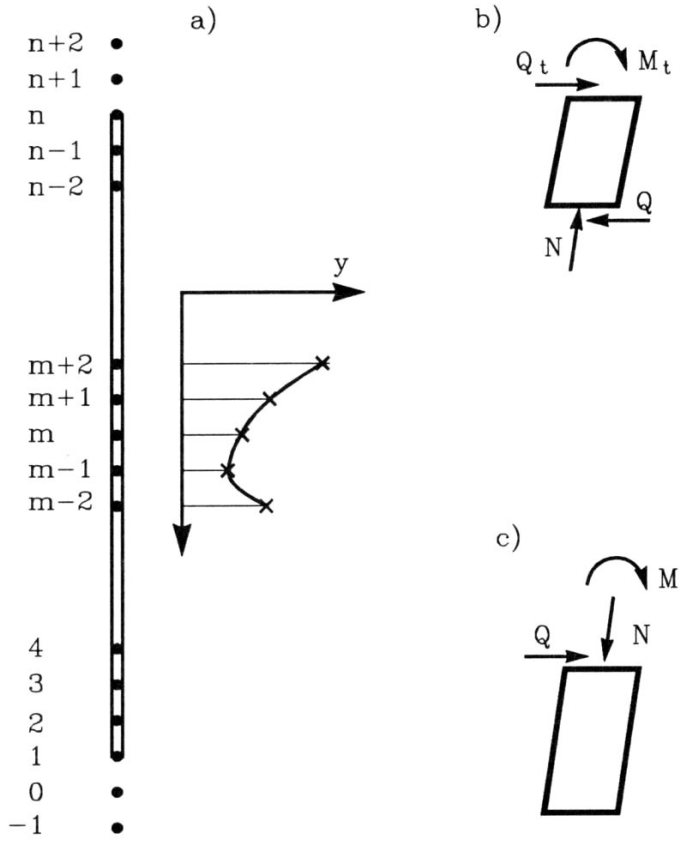

Figure 8.9: Finite difference method:
a) Discretization of piles in nodes b) equilibrium of top
c) equilibrium of bottom.

Boundary conditions at the bottom of a long pile

The moment can be assumed to be zero.

$$M = 0 \;\rightarrow\; \frac{\partial^2 w_y}{\partial z^2} = 0 \;\rightarrow\; w_{y,-1} - 2w_{y,0} + w_{y,+1} = 0 \qquad (8.13)$$

Horizontal shear is also assumed to be zero. Fig. 8.8 c) shows that

$$Q + N\,sin\left(\frac{\partial w_y}{\partial z}\right) = 0$$

or

$$EI\,\frac{\partial^3 w_y}{\partial z^3} + N\,\frac{\partial w_y}{\partial z} = 0$$

or

$$w_{y,-1} - 2w_{y,0} + 2w_{y,2} - w_{y,3} + \frac{Nh^2}{EI}\,(w_{y,0} - w_{y,2}) = 0 \qquad (8.14)$$

Boundary conditions at the top.

Horizontal load Q_t and moment M_t
Equilibrium of the top requires

$$M_t = EI\,\frac{\partial^2 w_y}{\partial z^2}$$

or

$$w_{y,n-1} - 2w_{y,n} + w_{y,n+1} = \frac{M_t}{EI} \cdot h^2 \qquad (8.15)$$

and

$$Q_t = Q + N\,\frac{\partial w_y}{\partial z}$$

or

$$w_{y,n-2} - 2w_{y,n-1} + 2w_{y,n+1} + w_{y,n+2} + \frac{Nh^2}{EI}\,(w_{Y,n-1} - w_{y,n+1})$$

$$= \frac{2Q_t h^3}{EI} \qquad (8.16)$$

The value of EI may be changed according to the connection to the upper part of the construction.

It is possible to have other boundary conditions as for instance horizontal load Q_t and slope of the pile at top level. New equations can be build up in a way similar to (8.15) and (8.16).

Chapter 9

References

ASTM D3441-79. (1979). *Deep, Quasi-Static, Cone and Friction Cone Penetration Tests of Soil.*

Azzouz, A.S. (1985). *The piezocone penetrometer.* MIT, Special Summer Course 1.60S. Recent Developments in Measurement and Modelling of Clay Behaviour for Foundation Design (6).

Baligh, M.M. (1960). *Interpretation of piezocone measurements during penetration.* MIT, Special Summer Course 1.60S. Recent Developments in Measurement and Modelling of Clay Behaviour for Foundation Design (7).

Baligh, M.M., Vivatrat, V., Ladd, C.C. (1980) *Cone penetration in soil profiling.* ASCE, JGED, GT4.

Battaglio, M., Maniscalco, R. (1983). *Il Pizocono. Esecuzione ed Interpretorione.* Atti del l'Istituto di Scienza delle Construzioni del Politecnico di Torino, No. 607. Torino.

Begeman, H.K.S. (1965). *The friction jacket cone as an aid in determining the soil profile.* Proc. 6th ICSMFE, Montreal, Vol. I.

Chow, Y.K. (1986). *Analysis of vertically loaded pile groups.* Int. Jour. for Numerical and Analytical Methods in Geomechanics. Vol. 10.

Dennis, N.D., Oleson, R.E. (1983). *Axial capacity of steel pipe lines in clay.* Proc. of the Conference on Geotechnical Practice in Offshore Engineering. Ed. Wright, S.G., ASCE, p. 370-388.

De Ruiter, J. (1987). *Offshore platforms and pipelines.* Series of Rock and Soil Mech., Vol. 13, chapter 3.

Durgunologu, H.T. and Mitchell, J.K. (1975). *Static penetration resistance of soils. I-II.* American Society of Civil Engineers. Conf. on In Situ Meas. of Soil Proporties. Releigh. North Carolina. Vol. 1.

Gwizdała, K., Jacobsen, M. (1990). *Nośność pali w spoistych. (Bearing capacity of piles in cohesive soils, undrained case).* Proc. IX Krajowa Konferencja Mechaniki Gruntów i Fundamentowania, Kraków, Poland. p. 113-117.

Hansen, J.B., Christensen, N.H. (1961). *The ultimate resistance of rigid piles against transversal forces.* The Danish Geotechnical Institute, Bulletin No. 12, Copenhagen 1963.

ISSMFE (1977). *Report of the Subcommittee on Standardization of Penetration Testing in Europe.* Proc. ICSMFE, Tokyo, V.3.

Jamiolkowski, M., Ladd, C.C., Germaine, J.T., Lancellotta, R. (1985). *New developments in field and laboratory testing of soils.* Proc. of the 11th Int. Conf. on Soil Mech. and Found. Eng., San Francisco, 12-16 August 1985.

Janbu, N. and Senneset, K. (1975). *Effective stress interpretation of in situ static penetration tests.* Proc. of the European Symposium on Penetration Testing, ESOPT 1, Stockholm, Sweden, Vol. 2.2.

Kerisel, J. (1961). *Fondations profondes en milieux sableu.* Proc. VI CSMFE, Vol. 2, Paris.

Kjekstad, O., Lunne, T., Clasen, C.J.F. (1978). *Comparison between in-situ cone resistance and laboratory strength for overconsolidated North Sea clays.* Marine Geotech., 3, No. 1.

Kulhawy, F.H. (1984). *Limiting tip and side resistance: fact or fallacy? Analysis and design of pile foundations.* Ed. Meyer, J.R., ASCE.

Lancellotta, R. (1983). *Analisi di Affidabilita in Ingegnena Geotecnica.* Atti Istituto Sienza Costnezioni. No. 625 - Politecnico di Torino.

Lunne, T. and Christoffersen, H.P. (1983). *Interpretation of cone penetrometer data for offshore sands.* Offshore Technology Conference, 15. Houston 1983. Proc. Vol. 1.

Lunne, T. Christoffersen, H.P. (1985). *Interpretation of Cone Penetrometer Data for Offshore Sands.* NGI Publication Nr. 156.

Lunne, T., Kleven, A. (1981). *Role of CPT in North Sea foundation engineering.* Symp. Cone Penetration Testing and Materials. ASCE Nat. Conv., St. Louis, MO.

Lunne, T., Lacasse, S. (1987). *Use of in situ tests in North Sea soil investigations.* NGI publications, Nr. 169.

Marsland, A. (1980). *The interpretation of in situ tests in glacial clays.* Proc. of a Conf. on Offshore site Investigation. Graham and Trotman Limited.

Matlock, H. (1970). *Correlations for Design of Laterally Loaded Piles in Soft Clay.* 2 Offshore Technology Conference, paper no 1204, p. 577-594.

McClelland, B. (1974). *Design of deep penetration piles for ocean structures.* Proc., Journal of the Geotechnical Engineering Division, ASCE, Vol. 100, No GT 7, p. 705-747.

McClelland, B., Focht, A.J., Emrich, J.W. (1969). *Problems in design and installation of offshore piles.* Journal of the SMFE ASCE, SM6, Vol. 95, No. SM6, November 1969.

Meyerhof, G.G. (1961). *The ultimate bearing capacity of wedge-shaped formations.* International Conference on Soil Mechanics and Foundation Engineering, 5. Paris. Proceedings, Vol. 2.

Meyerhof, G.G. (1976). *Bearing Capacity and Settlement of Pile Foundations.* Journal Geotechnical Div. Proc. ASCE, Vol. 102, No GT3, p. 197-228.

O'Neill, M.W., Reese, L.C. (1972). *Behaviour of bored piles in Beaumont Clay.* Jopurnal of Soil Mechanics and Foundations Division, ASCE, Vol. 98, No SM2, pp 195-213.

Peck, R.B., Hanson, W.F., Thornborn, T.H. (1953). *Foundation Engineering.* John Wiley & Sons, Inc. New York, 410 pp.

Poulus, H.G. (1982). *Single Pile Response to Cyclic Lateral Loading.* ASCE, Vol. 8, No GT3, pp 355-374.

Randolf, M.F. (1983). *Design consideration for offshore piles.* Proc. of the Conference on Geotechnical Practice in Offshore Engineering, Ed. Wright, S.G., ASCE, p. 422-439.

Robertson, P.K. and Campanella, R.G. (1983). *Interpretation of cone penetrometer test. Part I: Sand.* Canadian Geotechnical Journal. Vol. 20, No. 4.

Robertson, P.K. and Campanella, R.G. (1984). *Guidelines for use and interpretation of the electronics cone penetrometer test.* Soil Mech. Series No. 69. Dept. of C.E., The Univ. of British Columbia, Vancouver.

Sanglerat, G. (1972). *The Penetrometer and Soil Exploration.* Elsevier Publ. Co., Amsterdam.

Schmertmann, J.H. (1975). *Measurement of in situ shear strength. State-of-the-Art Report.* Proc. ASCE Specialty Conf. on in situ measurement of soil proporties. Raleigh. Vol. II.

Schmertmann, J.H. (1978). *Guidelines for cone penetration test: performance and design. United States.* Department of Transportation. Federal Highway Administration Offices of Research and Development. Washington, D.C. Report, TS-78-209.

Semple, R.M., Rigden, W.J. (1984). *Shaft capacity of driven pipe piles in clay. Analysis and design of pile foundations.* Ed. Meyer, J.R., ASCE.

Senneset, K., Janbu, N. (1984). *Shear strength parameters obtained from static cone penetration tests.* ASTM. Symp. San Diego, 1984.

Skempton, A.W. (1959). *Cast in-situ bored piles in London clay.* Geotechnique, Vol. 9, No 4-1959, pp. 73-153.

Tejchman, A., Gwizdała, K. (1988). *Comparative analysis of bearing capacity of large diameter bored piles.* Proc. of the 1st Int. Ged. Sem. on Deep Foundations on Bored and Auger Piles. Ghent 7-10 June 1988, p. 553-558.

Tejchman, A., Gwizdała, K. (1988). *Determination of the load - settlement curve for large diameter piles based on CPI results.* Proc. of the First International Symposium on Penetration Testing (ISOPT) – 1. Orlando, 20-24 March 1988, p. 1015-1020.

Tomlinson, M.J. (1957). *The Adhesion of Piles Driven in Clay Soils.* Proc. 4. Int. Conf. Soil Mech. and Found. Eng., Vol. 2, pp 66-71.

Vesic, A.S. (1975). *Principles of pile foundation design.* Soil Mechanics Series No 38.

Vijayvergiya, V.N., Focht, J.A. (1972). *A New Way to Predict Capacity of Piles in Clay.* 4. Offshore Technology Conference, Paper no 2939, pp. 465-475.

Woodward, R.J. Lundgren, R., Boitano, J.D. (1961). *Pile loading tests in stiff clays.* 5 Int. Conf. on Soil Mechanics and Foundation Engineering, Vol. 2, pp. 177-184.

Wroth, C.P. (1984). *The interpretation of in situ soil tests.* Draft of the written version of the 1984 Rankine Lecture.

Chapter 10

List of notations

Notations which are seldom used are defined in the text.

A_m	m^2	surface area of pile
A_P	m^2	tip area of pile
B	m	width of a footing
d	m	depth (length of pile in soil)
d_c	m	depth, critical
D	m	equivalent diameter or diameter
E	kPa	Youngs modulus
f	kPa	vertical shaft resistance
G	kPa	shear modulus
H	kN	horizontal resistance
I_D		density index
I_L		liquidity, index $I_L = 1 - I_P$
I_P		plasticity index
K		coefficient of earth pressure
K_o		coefficient of earth pressure at rest
L	m	total length of pile
M	kNm	moment
M_o	kPa	constrained modulus
N		bearing capacity factor
p	kPa	horizontal resistance
q	kPa	vertical point resistance

q_p	kPa	ultimate vertical point resistance
q_v	kPa	overburden pressure at pile tip level
Q	kN	total resistance
Q_m	kN	shaft resistance
Q_p	kN	point resistance
s	m	settlement of pile tip
s_u	kPa	undrained shear strength (Danish: c_u)
S		degree of saturation
u	kPa	pore pressure
w	m	movement
x, y	m	horizontal coordinates
z	m	vertical coordinate, positive downwards
α		coefficient of activated undrained shear strength
β		coefficient of activated drained shear stress
δ		friction at surface of pile
σ'_v	kPa	effective, vertical pressure
$\sigma_{v\,pc}$	kPa	effective, vertical preconsolidation pressure
OCR		Over Consolidation Ratio
w	%	water content
w_p	%	plasticity limit